

Molecular-dynamics study of structural-phase transitions. I. One-component displacement models

T. Schneider and E. Stoll

IBM Zurich Research Laboratory, 8803 Rüschlikon, Switzerland

(Received 21 July 1975)

Molecular-dynamics results simulating a canonical ensemble are presented and discussed for a two-dimensional one-component displacement model for ferrodistorptive and antiferrodistorptive structural-phase transitions. Our results include: (i) There is strong evidence that the system undergoes a continuous phase transition, except at the displacive limit. (ii) For three different sets of model parameters, the static critical exponents are found to be model parameters independent and consistent with those of the two-dimensional Ising model. (iii) The formation of clusters of locally ordered regions is demonstrated. (iv) Close to T_c and at the wave vector \vec{k}_c where the order-parameter susceptibility diverges, we observe a central peak around $\omega = 0$ in the dynamic form factor of the density fluctuations. (v) For wave vectors slightly away from \vec{k}_c the central peak splits into a double-peak structure, giving rise to a new excitation branch. (vi) The central peak and the new excitation branch are traced back to traveling cluster waves and their lifetime. (vii) The cluster dynamics is shown to dominate the critical slowing down.

I. INTRODUCTION

This paper is concerned with a two-dimensional one-component displacement model for ferrodistorptive and antiferrodistorptive structural-phase transitions. It may also be viewed as a set of harmonically coupled oscillators with quartic anharmonic and identical single-particle potentials. As the static properties are concerned, it is equivalent to a one-component continuous-spin model,¹ which reduces in a certain limit to the Ising model.²

Until recently, the molecular-dynamics technique, representing a brute-force numerical solution of the set of Newton equations associated with a given Hamiltonian,^{3,4} has not been applied to systems which might undergo phase transitions. Recently, we have undertaken such studies based on a one-component displacement model. It is the purpose of this paper to present and discuss the numerical results of this study. Some preliminary results have already been published elsewhere.⁵⁻⁹ The following main results are obtained.

(i) There is strong evidence that the system undergoes a continuous-phase transition, except at the displacive limit, where the order parameter vanishes already at zero temperature.

(ii) For three different sets of model parameters, the static critical exponents are found to be model-parameter independent and consistent with those of the two-dimensional Ising model.

(iii) The formation of clusters of locally ordered regions is demonstrated.

(iv) Close to T_c and at the wave vector \vec{k}_c where

the order-parameter susceptibility diverges, we observe a central peak around $\omega = 0$ in the dynamic form factor of the density fluctuations. In the displacive regime the central peak is distinct from the soft-mode doublet.

(v) For wave vectors slightly away from \vec{k}_c the central peak may split into a double-peak structure giving rise to a new excitation branch. The temperature at which this branch appears depends on the model parameters.

(vi) The central peak and the new excitation branch are traced back to traveling cluster waves and their lifetime.

(vii) The cluster dynamics is shown to dominate the critical slowing down.

The first main result is consistent with the exact proof of Kunz and Payandeh,¹⁰ stating that an ordered phase occurs up to and including some region of the displacive regime. The second confirms universality. The third result cannot be obtained by conventional phonon perturbation theory. In fact, it is a consequence of the strong nonlinearity. The fourth agrees with experiments. This central-peak phenomenon, first observed in SrTiO_3 , has received a variety of interpretations, which remain open to question.¹¹ The fifth result has not yet been observed in a real system. It is consistent, however, with particular solutions of the nonlinear equation of motion for the continuum limit, as considered by Krumhansl and Schrieffer.¹² They represent traveling cluster waves. The sixth agrees with the evidence that the central peak and the new excitations are due to the formation of clusters and their dynamics.

The one-component displacement model for

ferrodistortive and antiferrodistortive structural-phase transitions considered here, is described in Sec. II. Here we also define the Ising and displacive limit of this model as well as the order-disorder and displacive regime. To which regime the system belongs depends on the values of the model parameters chosen. Moreover, we present and discuss some exact relations and show that the displacive limit represents an isolated point where the critical exponents change discontinuously.

The molecular-dynamics technique is described in Sec. III, including the conventional microcanonical procedure^{3,4} and a new constant-temperature procedure, being more convenient to investigate critical properties. Here we also discuss how the static and dynamic properties can be calculated by assuming that the system is ergodic. In Sec. IV, we present some of our numerical results. They include:

(a) Static and critical properties, such as the temperature dependence of the order parameter, of the order-parameter susceptibility of the specific heat, and of the local mean-square displacement.

(b) The demonstration of the existence of clusters and of the temperature dependence of the cluster pattern.

(c) The temperature, wave-vector, and frequency dependence of the dynamic form factor of the density fluctuations and of the associated excitation spectrum. The temperature dependence of the spectral density of the time-dependent spatial-displacement autocorrelation function.

(d) It is shown that damped traveling cluster waves exist. The central peak and its splitting is then traced back to the cluster waves and their lifetime.

(e) The critical slowing down is shown to be dominated by the cluster dynamics. Section V contains our conclusions and some comments on related work, as well as on the experimental observability of the present results.

II. MODELS, REGIMES, AND EXACT RELATIONS

We consider the following two-dimensional lattice-dynamical model for a structural-phase transition:

$$\mathcal{H} = \frac{m}{2} \sum_{l,\kappa} (\dot{X}_{l\kappa}^2 + \dot{Y}_{l\kappa}^2) + \frac{A}{2} \sum_{l,\kappa} (X_{l\kappa}^2 + Y_{l\kappa}^2) + \frac{B}{4} \sum_{l,\kappa} (X_{l\kappa}^4 + Y_{l\kappa}^4) + \sum_{\substack{l',\kappa' \\ k',\kappa'}} V_{l\kappa l'\kappa'} X_{l\kappa} Y_{l'\kappa'} \quad (1)$$

κ labels the particles with mass m in the l th unit

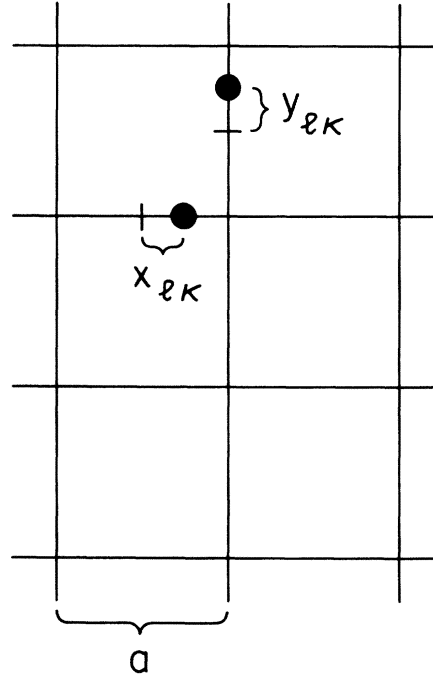


FIG. 1. Square reference lattice with lattice constant a . $X_{l\kappa}$ and $Y_{l\kappa}$ denote the displacements.

cell. $\dot{X}_{l\kappa}$, $X_{l\kappa}$, $\dot{Y}_{l\kappa}$, and $Y_{l\kappa}$ are velocity and displacement of the corresponding particle with respect to a square reference lattice with lattice constant a . It is important to note that a given particle can move only either in the X or Y direction (Fig. 1); m , A , B , and $V_{l\kappa l'\kappa'}$ are the model parameters. They are chosen in such a way that the mean displacement, representing the local order parameter does not vanish at low temperatures. Thus, the system is expected to undergo a structural-phase transition, which takes it from the low-temperature displacement configuration to a different high-temperature displacement pattern, where the mean local displacement vanishes.

A. Ferrodistortive models

To guarantee a ferrodistortive low-temperature phase, we choose

$$V_{l\kappa l'\kappa'} = \begin{cases} -C & \text{for nearest neighbors} \\ 0 & \text{otherwise.} \end{cases} \quad (2)$$

At zero temperatures, the properties of this phase can be calculated exactly within the framework of classical mechanics. In fact, by setting the force acting on the particles equal to zero, we find at $T=0$ for the local mean displacement

$$\langle X_{l\kappa} \rangle_{T=0} = \langle Y_{l\kappa} \rangle_{T=0} = (4C - A)/B. \quad (3)$$

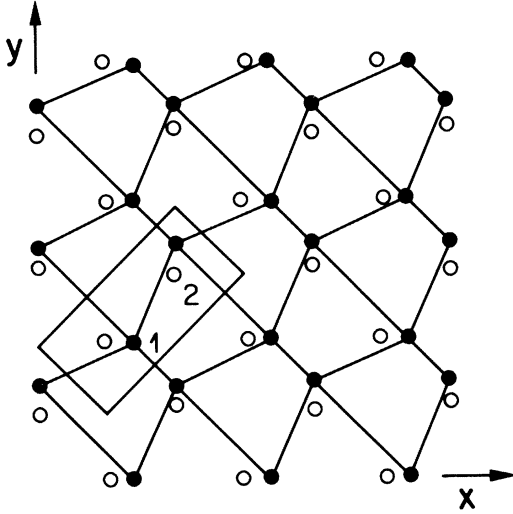


FIG. 2. Arrangement of the particles in the ferrodistorptive phase. Open circles represent lattice being equivalent to the mean arrangement in the high-temperature phase. The dots denote the mean positions in the ferrodistorptive phase. There are two particles per unit cell. κ takes on the value 1 only.

The corresponding ferrodistorptive arrangement of the particles is shown in Fig. 2. To guarantee that the energy of the ferrodistorptive phase is an absolute minimum and, moreover, that the system is stable, it is necessary that

$$4C - A > 0, \quad B > 0, \quad C > 0. \quad (4)$$

B. Antiferrodistorptive models

An antiferrodistorptive low-temperature phase is obtained by choosing

$$V_{i\kappa i'\kappa'} = \begin{cases} -C(-1)^{\kappa-\kappa'} & \text{for nearest neighbors} \\ 0 & \text{otherwise.} \end{cases} \quad (5)$$

At $T=0$, we find in analogy to Eq. (3),

$$\langle X_{i\kappa} \rangle = \left(\frac{4C - A}{B} \right)^{1/2} (-1)^\kappa. \quad (6)$$

The corresponding antiferrodistorptive arrangement of the particles is sketched in Fig. 3. The energy and stability requirements lead again to the conditions (4) for the model parameters. We note that the ferrodistorptive and antiferrodistorptive models may be mapped onto each other by means of the transformation

$$X_{i\kappa} \rightarrow (-1)^\kappa X_i, \quad (7)$$

where X_i is the ferrodistorptive local displacement

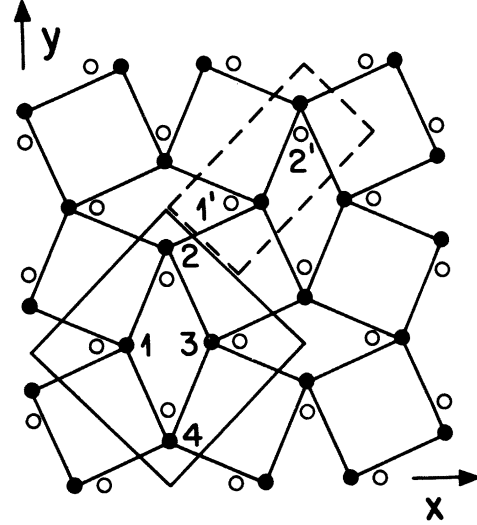


FIG. 3. Arrangement of the particles in the antiferrodistorptive phase. Open circles denote the reference lattice, being equivalent to the mean high-temperature pattern with two particles ($1'$ and $2'$) per unit cell. The dots characterize the mean displacement pattern in the antiferrodistorptive phase with four particles per unit cell. Particles 1 and 2 belong to sublattices with $\kappa=1$, and particles 3 and 4 to those with $\kappa=2$.

C. Order-disorder, displacive regime, Ising, and displacive limit

The structural-phase transitions associated with Hamiltonian (1) and the nearest-neighbor interactions defined in Eqs. (2) and (5) may be classified according to the form of the single-particle potential

$$\frac{1}{2}AX_{i\kappa}^2 + \frac{1}{4}BX_{i\kappa}^4, \quad (8)$$

appearing in the Hamiltonian. The choice $A < 0$ leads to a double-well single-particle potential, suggesting transitions of the order-disorder type. In fact, in the limit $A \rightarrow -\infty$, $B \rightarrow +\infty$ but $A/B = -1$, the zero-temperature values of the order parameters [Eqs. (3) and (6)] reduce to those of the spin- $\frac{1}{2}$ Ising ferromagnet or antiferromagnet, respectively. Moreover, in this limit the partition function reduces exactly to those of the corresponding Ising models.² As a consequence, the choice

$$A < 0, \quad B > 0, \quad C > 0 \quad (9)$$

leads to transitions of the order-disorder type and defines the order-disorder regime. In the displacive regime, where

$$A > 0, \quad B > 0, \quad C > 0, \quad (10)$$

the single-particle potential has a single minimum, consequently the low-temperature phase is stabilized only by the interaction. At the dis-

placive limit,

$$A = 4C, \quad (11)$$

the local order parameters [Eqs. (3) and (6)] vanish already at zero temperature. Figure 4 shows schematically the two regimes and their limits. For a more detailed discussion of these regimes and in particular for a discussion of the properties of the one-particle probability distribution we refer to Ref. 9.

D. Exact relations

In this section we derive some exact relations which turn out to be useful in the subsequent discussion. In doing so, we obtain from Eq. (1) for the equation of motion,

$$-m\ddot{X}_{i\kappa} = AX_{i\kappa} + BX_{i\kappa}^3 + 2 \sum_{i',\kappa'} V_{i\kappa i'\kappa'} Y_{i'\kappa'}. \quad (12)$$

Multiplying by $X_{i\kappa}$ we obtain for the kinetic energy per particle

$$2e_{\text{kin}} = k_B T = A \langle X_{i\kappa}^2 \rangle + B \langle X_{i\kappa}^4 \rangle + 2 \sum_{i',\kappa'} V_{i\kappa i'\kappa'} \langle Y_{i'\kappa'} X_{i\kappa} \rangle. \quad (13)$$

The potential energy per particle is, according to Eq. (1), given by

$$2e_{\text{pot}} = A \langle X_{i\kappa}^2 \rangle + \frac{1}{2} B \langle X_{i\kappa}^4 \rangle + 2 \sum_{i',\kappa'} V_{i\kappa i'\kappa'} \langle Y_{i'\kappa'} X_{i\kappa} \rangle. \quad (14)$$

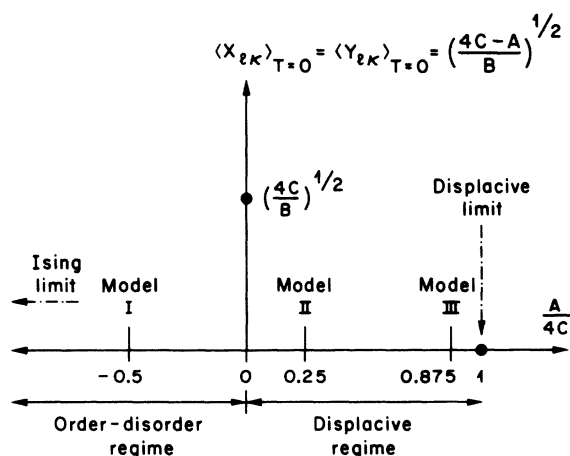


FIG. 4. Sketch of the order-disorder and displacive regime, including their limits for ferrodistorptive and antiferrodistorptive transitions. The ratios $A/4C = -0.5$, 0.25 , and 0.875 designate models I, II, and III, respectively, subsequently studied.

It then follows that

$$e_{\text{kin}} - e_{\text{pot}} = \frac{1}{4} B \langle X_{i\kappa}^4 \rangle = \frac{1}{2} k_B T - e_{\text{pot}} \quad (15)$$

and

$$e_{\text{tot}} = e_{\text{kin}} + e_{\text{pot}} = k_B T - \frac{1}{4} B \langle X_{i\kappa}^4 \rangle. \quad (16)$$

Equation (14) represents a particular form of the virial theorem, stating that the mean kinetic energy equals the virial, $\langle V \rangle$, where

$$\langle V \rangle = e_{\text{pot}} + \frac{1}{4} B \langle X_{i\kappa}^4 \rangle. \quad (17)$$

Equation (16) also allows expression of the specific heat in terms of the temperature derivative of the local quantity $\langle X_{i\kappa}^4 \rangle$, because

$$C = \frac{d}{dT} e_{\text{tot}} = k_B - \frac{B}{4} \frac{d}{dT} \langle X_{i\kappa}^4 \rangle. \quad (18)$$

To demonstrate that the displacive limit (see Fig. 4) represents an isolated point in the space of the model parameters, we consider the ferrodistorptive model. In this case and in the presence of a homogeneous external field h , the equation of motion (12) becomes, by invoking the interaction given by Eq. (2),

$$-m\ddot{X}_{i\kappa} = AX_{i\kappa} + BX_{i\kappa}^3 - 2C \sum_{m,\kappa} Y_{i+m\kappa} - h, \quad (19)$$

so that

$$\frac{4C-A}{B} \langle X_{i\kappa} \rangle + \frac{h}{B} = \langle X_{i\kappa}^3 \rangle. \quad (20)$$

At the displacive limit and $T = T_c = 0$, where the spontaneous local order parameter Eq. (3) vanishes, the equation of state (19) reduces to

$$h = B \langle X_{i\kappa} \rangle_{T=0}^3, \quad (21)$$

so that

$$\delta = 3. \quad (22)$$

This result holds for any dimension d . Emphasizing that for $d=2$ and the one-component order parameter considered here, δ is expected to be 15, the value of the two-dimensional Ising model, it becomes clear that the classical displacive limit represents an isolated point where critical exponents change discontinuously. For a more detailed discussion of the critical properties of the classical displacive regime and the associated crossover phenomenon, we refer to Ref. 13.

III. DYNAMICAL EQUATIONS AND METHOD OF SOLUTION

The dynamical equations required to describe the temporal evolution of our model systems are the coupled Newton equations. In the case of the

ferrodistortive model for particle lk we have [Eq. (19)]

$$-m\ddot{X}_{l\kappa} = AX_{l\kappa} + BX_{l\kappa}^3 - 2C \sum_{m,\kappa'} Y_{l+m\kappa'}. \quad (23)$$

From the computational point of view, it is convenient to choose the time unit in such a way that the mass of the particles is equal to one. Our calculations involve 3200 particles moving on a rigid reference lattice (Fig. 1), and subject to periodic boundary conditions. Starting from given initial conditions for the positions and velocities, the particles are then allowed to move, and their canonical variables ($X_{l\kappa}$, $\dot{X}_{l\kappa}$) are calculated according to a set of difference equations with a time increment. This set of difference equations approximates the set of Newton equations. To solve the difference equations, we used the predictor and corrector technique developed by Rahman and Gear.^{3,14} The time increment was chosen in such a way that the period of the oscillation with maximum frequency contained 70 time increments. The particles were placed initially at randomly chosen positions around their zero-temperature arrangement. The resulting displacements were restricted, however, to small values. Since this configuration leads to a small increase of the potential energy, the velocities quickly increased to a distribution characteristic to a low temperature. The system was then interrupted, and all velocities multiplied by a constant factor so that their distribution was characteristic for the desired temperature. To avoid drastic corrections we restricted the constant factor g to values $0.71 < g < 1.22$. Several repetitions of this procedure were required to bring the temperature close to the desired value. Thereafter, we used one of the following procedures: a microcanonical one, where the energy is a constant of motion, and a constant-temperature technique. Most calculations were carried out by means of the constant-temperature procedure.

A. Microcanonical procedure

In a microcanonical system, the energy is a constant of motion, so that

$$E_0 = E_{\text{kin}}(t) + E_{\text{pot}}(t) = \text{const} \quad (24)$$

and

$$E_{\text{kin}}[\frac{1}{2}V^2(t)] = E_{\text{kin}}[E_0 - E_{\text{pot}}(t)], \quad (25)$$

where V^2 denotes the mean-square velocity. Owing to the numerical noise in the integration procedure of the difference equations, condition (25) cannot be satisfied exactly. To overcome this

difficulty, we introduced a correction function $g(t)$ defined by

$$\begin{aligned} g^2(t)E_{\text{kin}}[\frac{1}{2}V^2(t)] &= E_{\text{kin}}[\frac{1}{2}g^2(t)V^2(t)] \\ &= E_{\text{kin}}[E_0 - E_{\text{pot}}(t)], \end{aligned} \quad (26)$$

so that

$$g^2(t) = [2/V^2(t)][E_0 - E_{\text{pot}}(t)]. \quad (27)$$

$g(t)V(t)$ represents the corrected mean velocity. Because $\eta(t)$, defined by $g(t) = 1 + \eta(t)$, turned out to be very small ($\approx 10^{-6}$) for sufficiently large systems, we performed this correction after any time increment. Temperature is inferred from the average value of the kinetic energy over the molecular-dynamics run; in a sufficiently long run

$$\langle V^2 \rangle = k_B T. \quad (28)$$

Temperature variations for a new calculation can be implemented by suitably modifying the velocities at the end of the previous run. A disadvantage of this procedure to investigate phase transitions arises from the relation between the mean-square fluctuations of the microcanonical ensemble and the susceptibilities of the canonical ensemble. To illustrate this point we note that¹⁵

$$\begin{aligned} (1/N)\langle \delta E_{\text{kin}}^2 \rangle_E &= (1/N)\langle \delta E_{\text{pot}}^2 \rangle_E \\ &= \frac{1}{2}k_B^2 T^2(1 - 1/2C_v), \end{aligned} \quad (29)$$

where C_v is the specific heat and $\langle \rangle_E$ denotes a microcanonical average. At $T = T_c$, the specific heat may diverge. Hence, the mean-square fluctuations tend to a constant value. Such a behavior is rather inconvenient to estimate critical exponents. The situation becomes even more severe, by considering the order-parameter susceptibility, which is given by¹⁵

$$N\langle \delta X \delta X \rangle_E = N\langle \delta X \delta X \rangle_T - \frac{T^2}{C_v} \left(\frac{\partial \langle X \rangle_E}{\partial T} \right)^2, \quad (30)$$

where the temperature dependence of $\langle X \rangle_E$ and $\langle \delta X \delta X \rangle_E$ has to be evaluated separately. Moreover, the specific heat C_v is given by Eq. (29) from which it is inconvenient to extract the critical behavior. In this case, it becomes clear that the microcanonical approach allows confirmation only of the inequality

$$\langle \delta X \delta X \rangle_T \langle \delta E_{\text{pot}} \delta E_{\text{pot}} \rangle_T \geq \langle \delta E_{\text{pot}} \delta X \rangle_T^2, \quad (31)$$

which leads to the Rushbrooke inequality¹⁶

$$\alpha + 2\beta + \gamma \geq 2. \quad (32)$$

B. Constant-temperature procedure

To overcome the difficulties associated with the conventional microcanonical procedure to estimate

critical properties, we developed a molecular-dynamics technique where the temperature is fixed at each time step. As a consequence the probability

$$dP_N(\dot{X}_1, \dots, \dot{X}_N; X_1, \dots, X_N) \\ = F_N(\dot{X}_1, \dots, \dot{X}_N; X_1, \dots, X_N) \prod d\dot{X}_i \prod dX_i \quad (33)$$

of finding the particles in the element $\prod d\dot{X}_i \prod dX_i$ near $\dot{X}_1, \dots, \dot{X}_N; X_1, \dots, X_N$ is determined by

$$F_N(\dot{X}_1, \dots, \dot{X}_N; X_1, \dots, X_N) \sim \delta\left(\frac{1}{N} \sum_i \dot{X}_i^2 - k_B T\right) e^{-\beta V}, \quad (34)$$

where V denotes the potential energy. This probability distribution leads to mean values equivalent to those of a canonical ensemble.

To fix the temperature at each time step, we rescaled the kinetic energy according to

$$g^2(t) E_{\text{kin}}\left[\frac{1}{2} V^2(t)\right] = E_{\text{kin}}\left[\frac{1}{2} g^2(t) V^2(t)\right] = \frac{1}{2} k_B T, \quad (35)$$

where $V^2(t)$ denotes the instantaneous mean-square velocity; $g(t)V(t)$ represents the corrected mean velocity. To keep the correction $\eta(t)$, defined by

$$g(t) = 1 + \eta(t), \quad (36)$$

small, we performed this rescaling of the kinetic energy in the predictor and the corrector step. Consequently, the kinetic energy is constant at each time step.

Assuming the system to be ergodic in the $(2N-1)$ -dimensional phase space (-1 because the temperature is fixed), time averages will coincide with the averages based on the probability given by Eqs. (33) and (34) characterizing a canonical ensemble. Concerning the dynamic properties, it is not clear, however, to what extent the fixed-temperature procedure affects the time-dependent correlation functions. To clarify this question and the accuracy of the integration procedure, we studied a set of 3200 coupled harmonic oscillations. The results, presented in Appendix A, demonstrate that the uncertainties due to the numerical noise and due to the fixed-temperature procedure do not lead to serious limitations. In particular we find that the associated damping and frequency shift is negligibly small.

C. Calculation of the static and dynamic properties

In all, over 20 000 time steps were expended in allowing the system to "age." After this interval, the subsequent period of 60 000–100 000 time steps was actually the time interval over which the time

averages reported below were calculated. We believe that the system had developed in time long enough to eliminate any effects due to the choice of the initial conditions.

Assuming the system to be ergodic, we performed, on this basis, time averages representing estimates for the ensemble averages. For example, the order parameter is given by

$$\langle X \rangle = \frac{1}{t_n - t_m} \int_{t_m}^{t_n} X(t) dt, \quad (37)$$

where

$$X = \frac{1}{2N} \sum_{i,k} (X_{i,k} + Y_{i,k}) (-1)^k. \quad (38)$$

A characteristic behavior of $X(t)$ is shown in Fig. 5 for $T < T_c$. Two time intervals may be distinguished: a first stage, in which the system relaxes to a metastable state. This metastable state may be so long-lived (τ_R , the second interval) that time averages, such as Eq. (37), become meaningful quantities. At τ_R , however, the system might undergo a "first-order transition." This behavior expresses the fact that in any finite system $\langle X \rangle$ vanishes at zero field. Nevertheless, as long as

$$\tau_R \gg t_n - t_m \quad (T < T_c) \quad (39)$$

and the interval $t_n - t_m$ is sufficiently long, reasonable time averages representing estimates for the infinite system can be performed. By approaching the transition temperature of the infinite system τ_R becomes shorter and τ_X increases. Consequently, condition (39) can no longer be fulfilled very close to T_c . The actual region depends, of course, on the number of particles and decreases with increasing N .

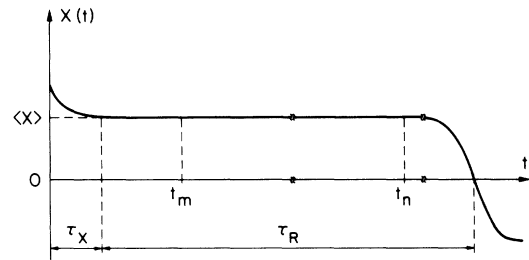


FIG. 5. Schematic time evolution of the order parameter $X(t)$. Two time intervals may be distinguished: (i) the decay to "equilibrium" τ_X which becomes critical, and (ii) this "equilibrium" state is a metastable state with lifetime τ_R , owing to the finite size of the system. Time averages representing estimates for the ensemble averages are taken from t_m to t_n . In practice, τ_R is accessible only close to T_c .

For $T > T_c$, condition (39) must be reversed:

$$\tau_R \ll t_n - t_m \quad (T > T_c). \quad (40)$$

In this case, $\langle X \rangle$ represents an estimate for $\langle X \rangle = 0$. In analogy to the situation below T_c , τ increases by approaching T_c and condition (40) can no longer be satisfied.

It now becomes evident that the molecular-dynamics technique provides a direct technique for estimating ensemble averages of an infinite system, except in a region around T_c . The actual extension of this region depends on the number of particles and the model parameters chosen. In the systems discussed subsequently it extends from $T/T_c \approx 0.98-1.06$.

This technique may also be used to estimate many other properties, such as the susceptibility

$$\chi = \frac{N}{k_B T} \frac{1}{t_n - t_m} \int_{t_m}^{t_n} [X(t) - \langle X \rangle]^2 dt \quad (41)$$

and the correlation functions

$$\hat{S}_{AA}(\vec{k}, t) = \frac{1}{S_{AA}(\vec{k}, t=0)} S_{AA}(\vec{k}, t), \quad (42)$$

where

$$\begin{aligned} S_{AA}(\vec{k}, t) &= \langle A(-\vec{k}, 0)A(\vec{k}, t) \rangle \\ &= \frac{N}{t_n - t - t_m} \int_{t_m}^{t_n - t} A(-\vec{k}, t')A(\vec{k}, t + t') dt'. \end{aligned} \quad (43)$$

A stands for

$$X(\vec{k}, t) = \frac{1}{N} \sum_{i, \kappa} [\exp(i\vec{k} \cdot \vec{R}_{i\kappa})][X_{i\kappa}(t) - \langle X_{i\kappa} \rangle], \quad (44)$$

$$\begin{aligned} \rho(\vec{k}, t) &= \frac{1}{N} \sum_{i, \kappa} \exp(i\vec{k} \cdot \vec{R}_{i\kappa} + \{X_{i\kappa}(t), 0\}) \\ &\quad - \langle \exp[i\vec{k} \cdot \vec{R}_{i\kappa} + \{X_{i\kappa}, 0\}] \rangle, \end{aligned} \quad (45)$$

$$\mu(\vec{k}, t) = \frac{1}{N} \sum_{L, \kappa} \exp(i\vec{k} \cdot \vec{R}_{L\kappa})[\mu_{L\kappa}(t) - \langle \mu_{L\kappa} \rangle], \quad (46)$$

$$\mu_{i\kappa} = \text{sgn} X_{i\kappa}. \quad (47)$$

Estimates for the associated spectral densities are obtained from

$$\hat{S}_{AA}(\vec{k}, \omega) = \frac{2}{S_{AA}(\vec{k}, t=0)} \int_0^{t_n - t_m} \cos \omega t S_{AA}(\vec{k}, t) dt. \quad (48)$$

Of the associated spectral densities, only $S_{\rho\rho}(\vec{k}, \omega)$ is accessible in a neutron-scattering experiment. $S_{\chi\chi}(\vec{k}, \omega)$ is closely related. $\mu(\vec{k}, t)$ denotes the fluctuations of the Ising variable, characterizing

the cluster dynamics. A cluster consists of a locally ordered region, with $\mu_{i\kappa}$ identical or opposite to those at $T=0$.

Because $t_n - t_m$ is finite, $\hat{S}_{AA}(\vec{k}, t)$ as defined by Eq. (43) will deviate from the exact value by $\delta \hat{S}_{AA}(\vec{k}, t)$. This deviation increases with t , whereas $\hat{S}_{AA}(\vec{k}, t)$ decreases. Consequently, the relative error increases with t . To reduce the associated uncertainties, we replaced $\hat{S}_{AA}(\vec{k}, t)$ in Eq. (48) by

$$S_{AA}(\vec{k}, t) \exp\{-[t/\tau_d(\vec{k})]^2\}. \quad (49)$$

$\tau_d(\vec{k})$ leads to an additional damping. To extract the low-frequency structure of $S_{AA}(\vec{k}, \omega)$, $\tau_d(\vec{k})$ was chosen according to

$$\tau_d(\vec{k}) \gg \tau_{AA}(\vec{k}), \quad (50)$$

where

$$\tau_{AA}(\vec{k}) = \hat{S}_{AA}(\vec{k}, \omega=0). \quad (51)$$

$\tau_{AA}(\vec{k})$ is the relaxation time characterizing the critical slowing down (see Sec. IV E). As a consequence, the resulting spectral densities (48) represent a folding between a resolution function [second term in Eq. (49)] and the true function. Condition (50) guarantees, however, that the low-frequency structure in $S_{AA}(\vec{k}, \omega)$ will be resolved.

For high frequencies, condition (50) has been replaced by

$$\tau_d(\vec{k}) \gg 1/\Gamma(\vec{k}), \quad (52)$$

where $\Gamma(\vec{k})$ denotes the half-widths of the peaks in this frequency region.

In view of the reasons discussed in Sec. III, we adopted the constant-temperature procedure to evaluate the time averages. Consequently, our susceptibilities represent estimates for the isothermal ones, whereas the time-dependent correlation function should be ensemble independent.¹⁵

IV. NUMERICAL RESULTS

A. Static properties

In this section we report some estimates based on three models, differing in the parameters chosen. These parameters are listed in Table I, and apply to both the ferrodistorptive and antiferrodistorptive systems. In fact, these systems may be mapped onto each other. Model I corresponds to an order-disorder system and models II and III belong to the displacive regime. From Fig. 4, it is seen that model III is close to the displacive limit.

We note that the partition function associated with the Hamiltonian (1) and the interaction terms specified in Eqs. (2) and (5) reduces in the limit $A = -\infty, B = +\infty$ but $A/B = -1$ to that of the Ising ferromagnet and antiferromagnet, respectively.² In-

voking the universality hypothesis, one expects therefore that the static critical exponents of all three models should be equal to the corresponding exponents of the spin- $\frac{1}{2}$ Ising model except at the

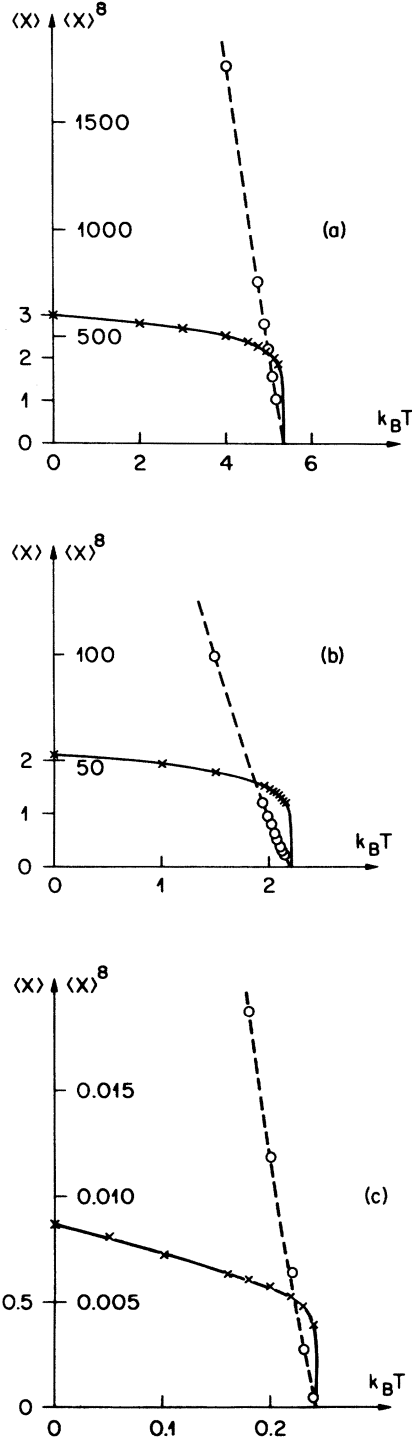


FIG. 6. Calculated temperature dependence of the order parameter $\langle X \rangle$ and $\langle X \rangle^8$: (a) model I; (b) model II; (c) model III.

displacive limit [Eq. (11)], representing an isolated point [see Eq. (22)].

In this case, it makes sense to plot the order parameter as a function of T to the power eight and the isothermal susceptibility as $\chi_T^{-4/7}$. In fact, from the two-dimensional Ising model one expects the behavior¹⁶

$$\langle X \rangle = G_X (T_c - T)^{1/8}, \quad (53)$$

$$\chi_T = G_\chi |T_c - T|^{-7/4}. \quad (54)$$

In Fig. 6 we summarized the calculated temperature dependence of the order parameter. From the $\langle X \rangle^8$ plot, it is seen that our results are consistent with the Ising power law. The amplitude G_X , however, is seen to decrease by approaching the displacive limit. From the $\langle X \rangle^8$ plot, we also estimated the critical temperatures listed in Table I.

Figure 7 shows the calculated temperature dependence of the isothermal susceptibility. In models I and II, we find below T_c consistency with the Ising power law. Above T_c and in particular in model III, the critical region is found to be inaccessibly small, however.

Finally, we turn to the temperature dependence of the specific heat, shown in Fig. 8. Obviously, our results are consistent with the logarithmic singularity characteristic for the two-dimensional Ising model. We find, however, a reduction of the amplitude by approaching the displacive limit.

Summarizing these results, we note: (a) the universality hypothesis is consistent with our numerical results; (b) the amplitudes of the power laws are found to be model parameter dependent; and (c) continuous-phase transition are expected even in the displacive regime and close to the displacive limit (Fig. 4).

Finally, we turn to the local mean-square displacement being a relevant quantity in the self-consistent phonon approximation (Appendix B). Moreover, this quantity is also related to the linewidth broadening of the paramagnetic resonance on paramagnetic ions, randomly distributed in systems undergoing structural-phase transitions.¹⁷

TABLE I. Model parameters for models I-III. T_c has been estimated from the calculated temperature dependence of the order parameter. $\langle X \rangle_{T=0}^2$ denotes the order parameter squared at zero temperature, given by Eqs. (3) and (6).

Model	A	B	C	A/4C	$k_B T_c$	$\langle X \rangle_{T=0}^2$
I	-1	$\frac{1}{3}$	$\frac{1}{2}$	-0.5	5.3 ± 0.05	9
II	$\frac{1}{2}$	$\frac{1}{3}$	$\frac{1}{2}$	+0.25	2.2 ± 0.02	4.5
III	$\frac{7}{4}$	$\frac{1}{3}$	$\frac{1}{2}$	+0.875	0.245 ± 0.003	0.75

In fact, close to T_c the critical part of the line-width squared is expected to be proportional to $\langle(\delta X_{i\kappa})^2\rangle$. In Fig. 9(a) we show the calculated temperature dependence of $\langle X_{i\kappa}^2\rangle$ and $\langle(\delta X_{i\kappa})^2\rangle = \langle X_{i\kappa}^2\rangle - \langle X_{i\kappa}\rangle^2$ in model I. It is seen that $\langle X_{i\kappa}^2\rangle$ tends to a constant value at T_c and is, consequently, uncritical. As a consequence, this also holds for $\langle(\delta X_{i\kappa})^2\rangle$, as pointed out by von Waldkirch *et al.*¹⁷ The temperature derivative of this quantity $\langle(\delta X_{i\kappa})^2\rangle$ is singular however, [see Fig. 9(b)] and would allow an independent determination of the critical exponent β . Similarly, the temperature derivative of $\langle X_{i\kappa}^4\rangle$ would also be singular [see Eq. (18)].

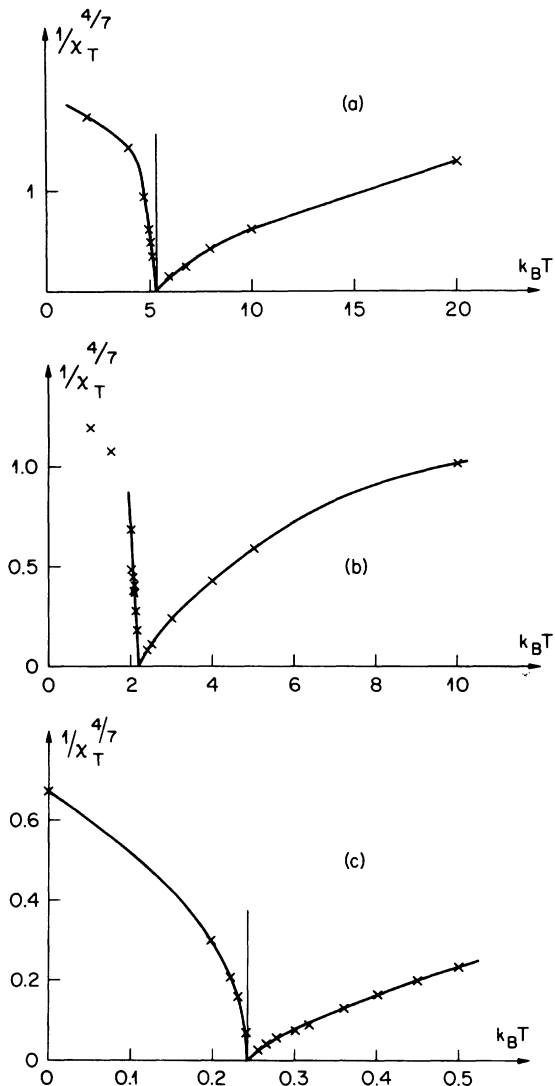


FIG. 7. Calculated temperature dependence of the isothermal susceptibility χ_T : (a) model I; (b) model II; (c) model III.

B. Formation of cluster

An interesting observation was made by analyzing the time evolution of the model systems. In fact, it turned out that clusters are formed, representing particles connected by nearest-neighbor bonds and having local instantaneous order parameters with a sign opposite to that expected from zero temperature.

Figure 10 shows snapshots of cluster configurations taken at various temperatures in model III.

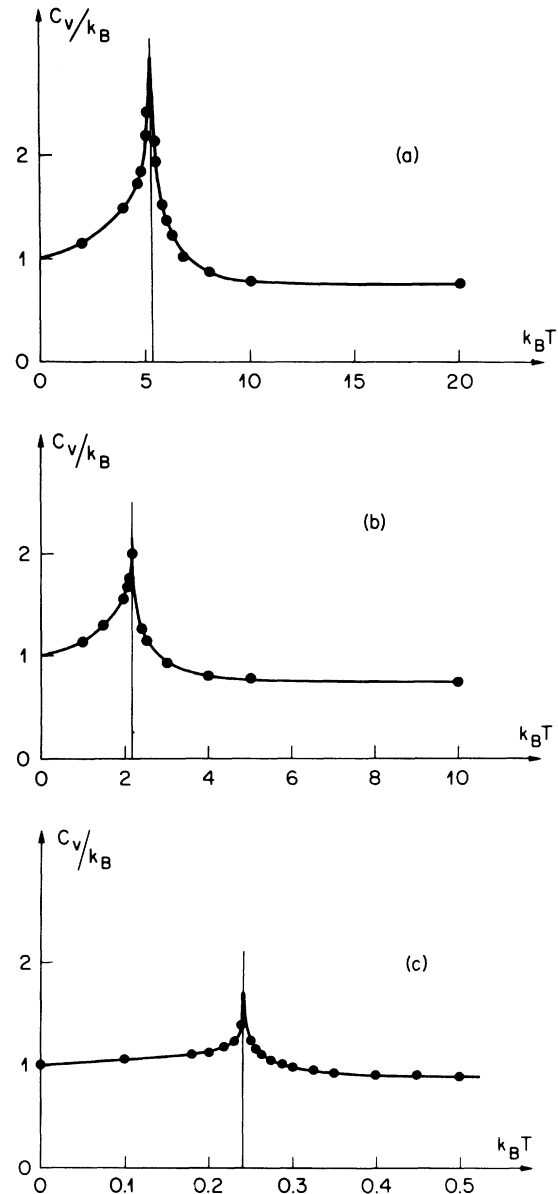


FIG. 8. Calculated temperature dependence of the isothermal specific heat C_T : (a) model I; (b) model II; (c) model III.

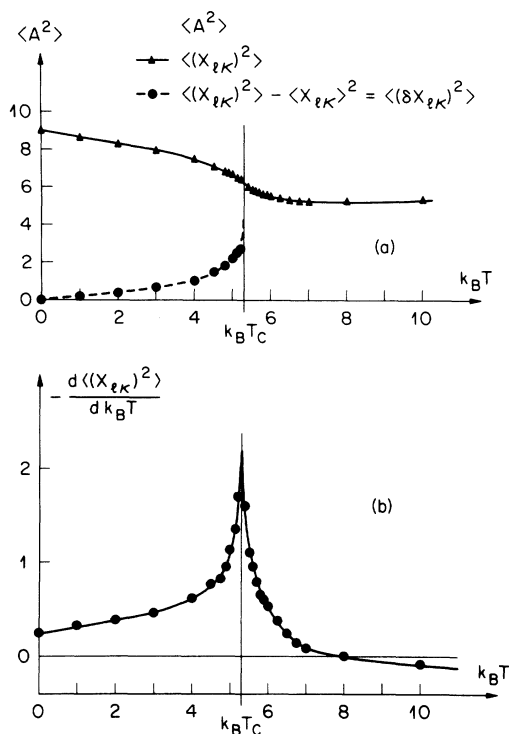


FIG. 9. (a) Temperature dependence of $\langle X_{iK}^2 \rangle$ and $\langle (\delta X_{iK})^2 \rangle$ in model I (Table I); (b) Temperature dependence of $d\langle X_{iK}^2 \rangle / dT$ in model I.

By approaching T_c the cluster size is seen to increase. Above T_c , the number of clusters with positive and negative local order parameters remains of course equal. It is seen, however, that above T_c , the clusters become smaller with increasing temperature as one expects.

The formation of these clusters and of the associated cluster walls has important consequences. In fact, the existence of these clusters reveals that a given particle not only vibrates around a mean position, but that this mean position itself is tied to the cluster dynamics. Such complicated motion cannot, of course, be treated within the framework of the conventional theory of lattice dynamics, assuming well-defined equilibrium positions.

It should also be noted that the cluster border is sharp only in the Ising limit (Fig. 4). Otherwise, the local displacements are continuous variables ($-\infty \leq X_i \leq +\infty$). Thus, the cluster is expected to become increasingly blurred by approaching the displacive limit. A preliminary analysis reveals, however, that this smearing out of the cluster border becomes effective only close to the displacive limit.

In the spirit of the Chinese proverb "A picture says more than a thousand words," we should like to mention that the formation of clusters and their dynamics has also been demonstrated by means of a motion picture.¹⁸

C. Spectral densities and excitation spectrum

To investigate the excitation spectrum we calculated various spectral densities, defined by Eq. (48). Of particular interest is the dynamic form factor $S_{\rho\rho}(\vec{k}, \omega)$ which can be measured by the neutron-scattering technique. Provided that phonons are well-defined excitations, they appear in $S_{\rho\rho}(\vec{k}, \omega)$ at fixed wave vector, as a narrow peak. Until recently, it was believed that the critical dynamics of structural-phase transitions is dominated by a soft phonon whose frequency decreases as the transition temperature is approached from above or below and vanishes at T_c . This soft-mode concept, implicitly suggested by the Lyddane-Sachs-Teller relation, has been developed by Landauer, Cochran, and Anderson.¹⁹ New observations have indicated, however, that the dynamics of these transitions might be more complicated and also more interesting than previously assumed. In fact, neutron-scattering²⁰ and EPR measurements^{17,21,22} have shown in addition to the soft-mode peaks, the appearance of a central component around $\omega = 0$ in the dynamic form factor. Up to now, it has not been possible, however, to resolve this central peak by means of the neutron-scattering technique and to study its temperature dependence. Nevertheless, the experiment indicates that the central peak seems to be distinct from the soft-mode doublet that is also present close to T_c , either strongly damped or overdamped for those wave vectors where the central peak is strong.²⁰ This phenomenon has received a variety of interpretations which remain open to question.^{11,23} The microscopic attempts have been based on diagrammatic techniques, familiar from phonon hydrodynamics, by summing up some class of graphs in order to obtain additional structure in $S_{\rho\rho}(\vec{k}, \omega)$. Besides the fact that these calculations can only be performed under hardly controllable approximations, one also misses a clear physical picture of the mechanism producing the central peak.

On the other hand, molecular-dynamics calculations also revealed the occurrence of a central peak in model systems, at least undergoing structural-phase transitions.^{5,6,8} This central peak was not only resolved but also traced back to the formation of clusters and their dynamics.^{5,6,8} In this section, we present additional results and discuss them in more detail.

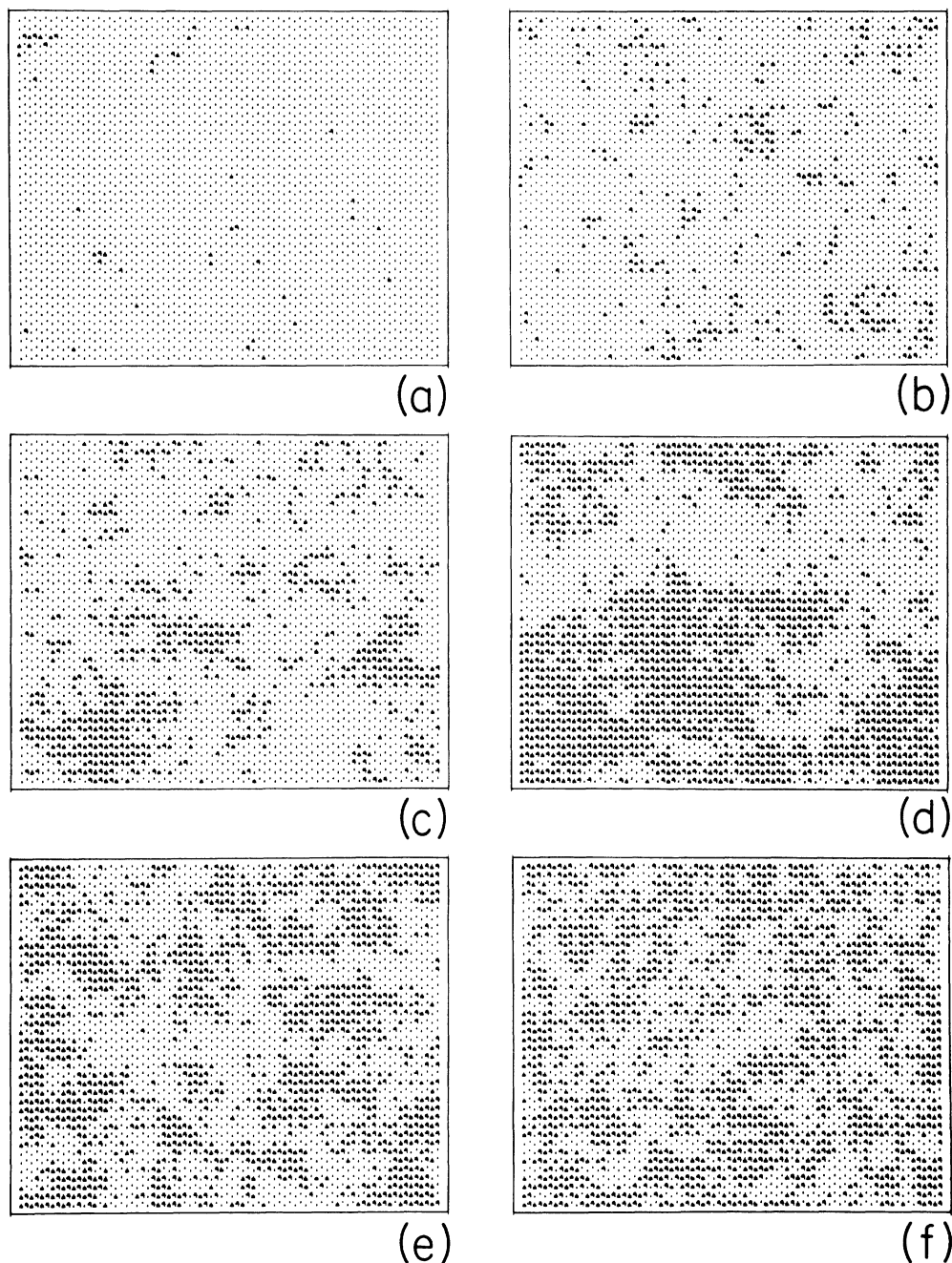


FIG. 10. Snapshots of instantaneous cluster configurations in model III ($k_B T_c = 0.245$). Dark points designate particles whose local order parameter have a sign opposite to that expected from $T = 0$. Brighter points denote the particles whose local order parameter have a sign identical to that at $T = 0$: (a) $k_B T = 0.1$; (b) 0.22; (c) 0.24; (d) 0.25; (e) 0.3; (f) 0.8.

In doing so we first introduce the Brillouin-zone scheme for the high- and low-temperature phases shown in Fig. 11. Here, we present our results in the zone scheme appropriate for the antiferro-distortive models. These results can easily be transformed to the ferrodistorptive case by the

following transformation:

$$\begin{aligned} (\pi/a)(1, 1) &\leftrightarrow (\pi/a)(2, 0), \\ (\pi/a)(3, 1) &\leftrightarrow (\pi/a)(4, 0). \end{aligned} \quad (55)$$

Moreover, it should be recalled that in the ferro-

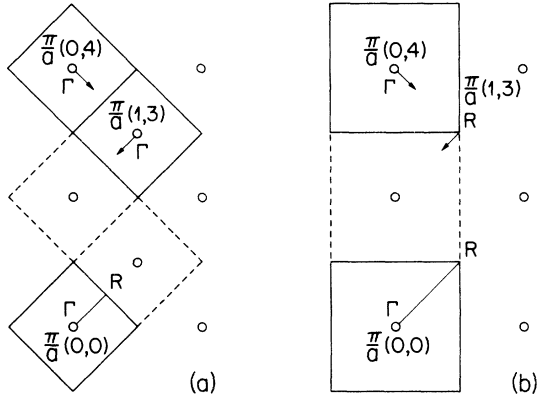


FIG. 11. Brillouin zones of an (a) antiferrodistortive and (b) ferrodistortive model in the low-temperature phase. Above T_c , the zone scheme is given by (b) in both cases.

distortive case, with two particles per unit cell, there are only two phonon branches in the low-temperature phase.

Let us now start with the discussion of the dynamic form factor of model III, being close to the displacive limit (Fig. 4). In Fig. 12(a) we show some results of the calculated $S_{\rho\rho}(\vec{k}, \omega)$ at $k_B T = 0.24$, being close but below $k_B T_c = 0.245$ (Table I). At $(3, 1)$ the spectrum is dominated by a central peak. We also observe, however, the soft-mode peak marked by 2. It is important to note that the half-width of this central peak is several orders of magnitude larger than the inverse damping constant arising from the numerical noise and from the constant-temperature procedure (see Appendix A) and smaller than $1/\tau_d(\vec{k})$ [Eq. (50)]. Consequently, this central peak is real and has been resolved. Slightly away from $(3, 1)$, the central peak is seen to split into a double-peak structure, appearing in addition to the soft-mode resonance. The k dependence of the norm $S_{\rho\rho}(\vec{k}, t=0)$ reveals, however, that the strength of the split central peak decreases very fast with \vec{k} values taken relative to $(3, 1)$. By plotting the peak maxima of $S_{\rho\rho}(\vec{k}, \omega)$ for various \vec{k} vectors parallel to $(1, 1)$ we find the dispersion relation shown in Fig. 12(b). There are four phonon branches. For comparison we included the prediction of the self-consistent phonon approximation (SCPA) (Appendix B), where $(X_{1\kappa}^2)$ was determined by means of molecular dynamics. From Fig. 12(b), it is seen that SCPA leads to a reasonable description of the phonon frequencies except in a small-wave-vector region of the soft phonon branch.

More exciting is the appearance of an additional excitation branch, originating from the splitting of the central peak. This branch is well defined only up to a cut-off wave vector.

Above T_c , where only two phonon branches are expected, we found a similar behavior, as demonstrated by Fig. 13. In fact, at $(3, 1)$ there is a resolved central peak and a weak soft-mode resonance. Slightly away from $(3, 1)$, the central peak is again seen to split into a double-peak structure, giving rise to the new excitation branch [Fig. 13(b)].

By going further away from T_c , the central-peak intensity is found to decrease, whereas the soft-mode resonance intensity increases. In this temperature region, we found no evidence for the new excitation branch.

In model I, belonging to the order-disorder regime (Fig. 4), the phonons turned out to be not well defined for temperatures slightly different from $T=0$. This fact is also seen in Fig. 14, where we plotted the calculated $S_{\rho\rho}(\vec{k}, \omega)$ for wave vectors \vec{k} parallel to $(1, 1)$. The temperature $k_B T$

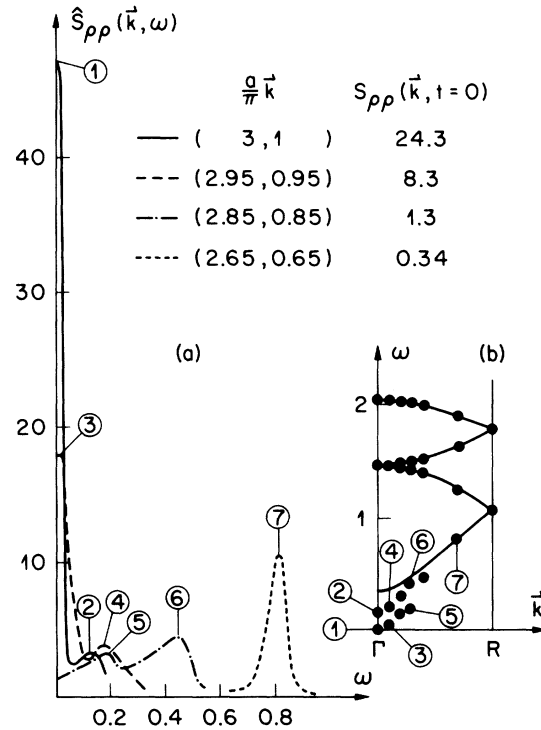


FIG. 12. (a) Frequency dependence of $\hat{S}_{\rho\rho}(\vec{k}, \omega)$ at some fixed \vec{k} values close to $(\pi/a)(3, 1)$ in model III at $k_B T = 0.24$, being close but below $k_B T_c = 0.245$. The peak maxima 2, 4, 6, and 7 are due to the conventional soft mode. The peaks 3 and 5 represent evidence for the new excitation branch. (b) Phonon dispersion and dispersion of the new excitation branch in model III at $k_B T = 0.24$ for \vec{k} parallel to $(1, 1)$. The numbers label corresponding peak maxima in Fig. 12(a). The solid curve was obtained by means of a SCPA (see Appendix B).

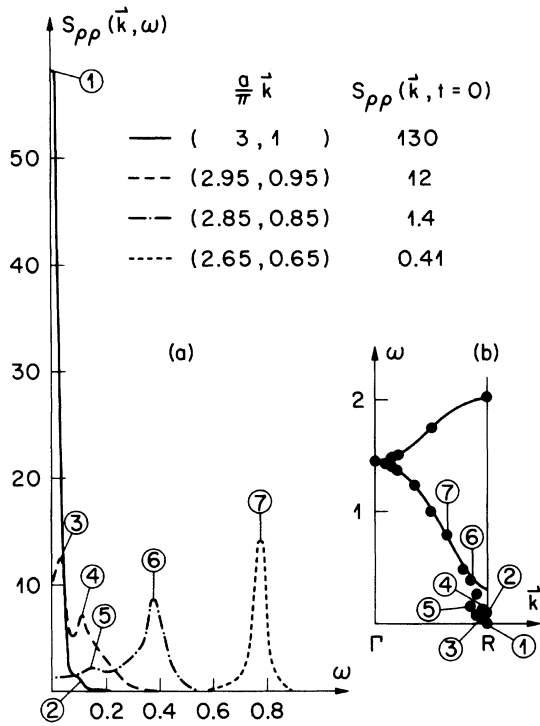


FIG. 13. (a) Frequency dependence of $\hat{S}_{\rho\rho}(\vec{k}, \omega)$ at some fixed \vec{k} values close to $(\pi/a)(3, 1)$ in model III at $k_B T = 0.26$, being close but above T_c . The peak maxima 2, 4, 6, and 7 are due to the conventional soft mode. The maxima 3, 4, and 5 represent evidence for the new excitation branch. (b) Phonon dispersion and dispersion of the new excitation branch in model III at $k_B T = 0.26$. The numbers label corresponding peaks in Fig. 13(a). The solid curve was obtained on the basis of a SCPA (see Appendix B).

$= 5.7$ is above but near to $k_B T_c = 5.3$. Obviously the spectrum is dominated by the central peak only and there is no evidence for phonon resonances. Moreover, the central peak does not split for wave vectors slightly away from $(3, 1)$. Consequently, there is also no evidence for the new excitation branch.

To clarify the occurrence of the new excitation branch in this model belonging to the order-disorder regime, we also studied the temperature dependence of $S_{\rho\rho}(\vec{k}, \omega)$. From Fig. 15, it is seen that at $k_B T = 8$, being above $k_B T_c = 5.3$, the central peak splits into a double-peak structure for wave vectors slightly away from $(3, 1)$. Consequently, the new excitation branch appears again. For lower temperatures, however, we found no evidence for such a splitting. At higher temperatures, on the other hand, the detection of a possible splitting became difficult owing to the small intensity of the central peak.

Because the new excitation branch evolves from

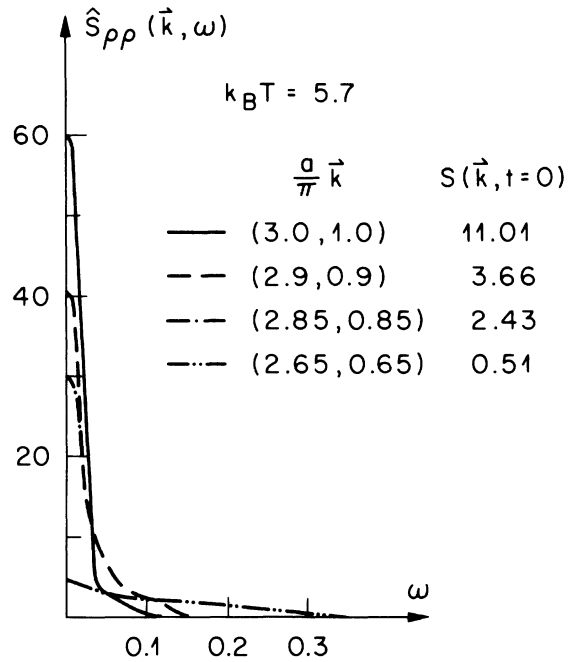


FIG. 14. Frequency dependence of $\hat{S}_{\rho\rho}(\vec{k}, \omega)$ at some fixed \vec{k} values close to $(3, 1)$ in model I at $k_B T = 5.7$, being above but close to $k_B T_c = 5.3$ (Table I).

the central peak by varying the wave vector, it is suggestive that there is a common underlying mechanism. To substantiate this conjecture, we also calculated the dynamic form factor of the

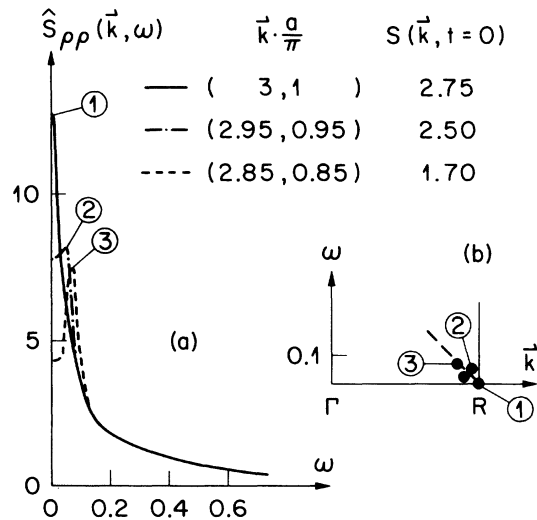


FIG. 15. (a) Frequency dependence of $\hat{S}_{\rho\rho}(\vec{k}, \omega)$ at some fixed \vec{k} values close to $(3, 1)$ in model I, at $k_B T = 8$ ($k_B T_c \approx 5.3$). (b) Dispersion relation of the new excitation branch. The numbers label corresponding peaks in Fig. 15(a).

Ising variable [Eqs. (42), (46), and (48)] characterizing the cluster dynamics. It was found that both the central peak and the new excitation branch also appear in this spectral density at corresponding temperatures. Therefore, one will be led naturally to the conclusion that both phenomena are due to the cluster dynamics. The appearance of the new excitations, however, is not only tied to the presence of a central peak but also depends on the model parameter chosen. In fact, in model III they appeared close to, but above and below T_c , whereas in model I, they are visible only above T_c .

This may be understood by recalling again that the new excitation branch arises from the collective "flipping" of the particles from one effective potential well to the other. This collective "flipping" can be effective only if $k_B T$ exceeds the depth of these wells. This depth is given by $\frac{1}{4}B[(4C-A)/B]^2$, and corresponds to the temperatures $k_B T = 0.047$ in model III and $k_B T = 6.75$ in model II (see Table I). Obviously, this argument fits with the numerical results, revealing that the new excitations appear in model III above and below $k_B T_c = 0.245$, and in model I above $k_B T_c = 5.3$ only.

It is interesting to note that our central-peak results are consistent with a Lorentzian frequency distribution. In fact, the half-width $\Delta\omega$ satisfies [see Figs. 12(a), 13(a), 14, and 15],

$$\Delta\omega\hat{S}_{pp}(\vec{k}_c, \omega=0) \approx 1, \quad (56)$$

where \vec{k}_c denotes the wave vector where the order-parameter susceptibility diverges.

Finally, we turn to the spectral density of the time-dependent spatial displacement autocorrelation function, defined by

$$\hat{S}_A(\omega) = 2 \int_0^{t_n - t_m} \hat{S}_A(t) \cos \omega t dt, \quad (57)$$

where

$$\hat{S}_A(t) = \frac{\langle X_{I\kappa}(0)X_{I\kappa}(t) \rangle - \langle X_{I\kappa} \rangle^2}{\langle X_{I\kappa}^2 \rangle - \langle X_{I\kappa} \rangle^2}, \quad (58)$$

$$\begin{aligned} &\langle X_{I\kappa}(0)X_{I\kappa}(t) \rangle \\ &= \frac{1}{t_n - t - t_m} \int_{t_m}^{t_n - t} X_{I\kappa}(t')X_{I\kappa}(t + t') dt'. \end{aligned} \quad (59)$$

This spectral density is related to the linewidth broadening of the paramagnetic resonance of paramagnetic ion centers, randomly distributed in systems undergoing structural-phase transitions.^{17,21} In Fig. 16 we plotted the frequency dependence of this spectral density for various temperatures in model II. It is seen that also in this function, a central peak appears by approaching $k_B T_c = 2.2$ from above or below and that its half-

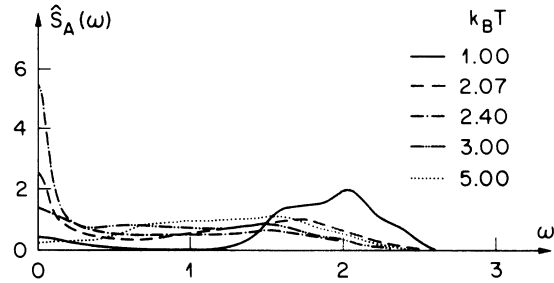


FIG. 16. Frequency dependence of the spectral density of the local displacement fluctuations [Eq. (57)] in model II (Table I) at various temperatures ($k_B T_c \approx 2.2$).

width decreases. Another important feature is that close to T_c (see $k_B T = 2.4$) two frequency regimes may be distinguished. A low-frequency regime, dominated by a central peak which characterizes the cluster dynamics. Above some cut-off frequency, there is some smooth background arising from the fast motions. The distinction between these slow- and fast-motion regimes is also seen in Fig. 17, where the time dependence of the spatial autocorrelation function is shown. We note that the existence of these two regimes plays a crucial role in the interpretation of the linewidth broadening of the paramagnetic resonance as a tool to investigate dynamic critical phenomena.^{17,21}

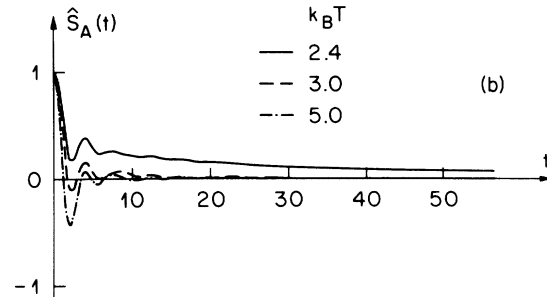
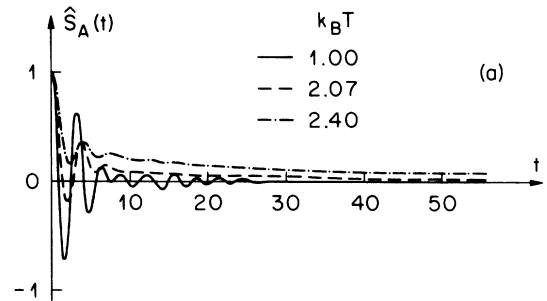


FIG. 17. Time dependence of the local displacement correlation function in model II at various temperatures ($k_B T_c \approx 2.2$): (a) $k_B T = 1, 2.07, 2.4$; (b) $k_B T = 2.4, 3, 5$.

More recently, it even became possible to account quantitatively for the EPR line anisotropy for $T_c \leq T \leq 300^\circ\text{K}$ in SrTiO_3 , by assuming a central peak and a smooth high-frequency background.²² Moreover, it has been shown that the central peak in $S_A(\omega)$ dominates the secular relaxation, and the smooth background the non-secular relaxation.²²

D. Cluster waves

Nonlinear wave processes are involved in phenomena occurring in many scientific areas.²⁴⁻²⁶ It suffices to mention elastic properties of media, ergodicity, surface waves in liquids, propagation of magnetic flux on a Josephson line, wave motion in a plasma, nonlinear optic and electrodynamics, theory of elementary particles, etc.

The formation of clusters and their dynamics (Sec. IV B) revealed that strong nonlinearity also plays an important role in systems undergoing structural-phase transitions. These findings may also be understood by considering particular so-

lutions of the associated classical equations of motion. In fact, Krumhansl and Schrieffer¹² found, by studying a strongly anharmonic chain, particular solutions representing cluster walls which cannot be described by the conventional phonon perturbation expansions. At low temperatures, they found that the exactly calculated static properties agree with those found from a phenomenological model in which both phonons and clusters are included as elementary excitations.

To demonstrate the relevance of these cluster excitations and to clarify their relation to the central-peak phenomenon and to the new excitation branch, we also analyzed our results from this point of view. In doing so we considered only small ω and k values to calculate

$$X_i^*(t) = \text{Re} \sum_{|k_x| \leq |k_{xc}|} \sum_{|\omega| \leq \omega_c} X(\vec{k}, \omega) \times e^{-i(\vec{k} \cdot \vec{R}_i - \omega t)}. \quad (60)$$

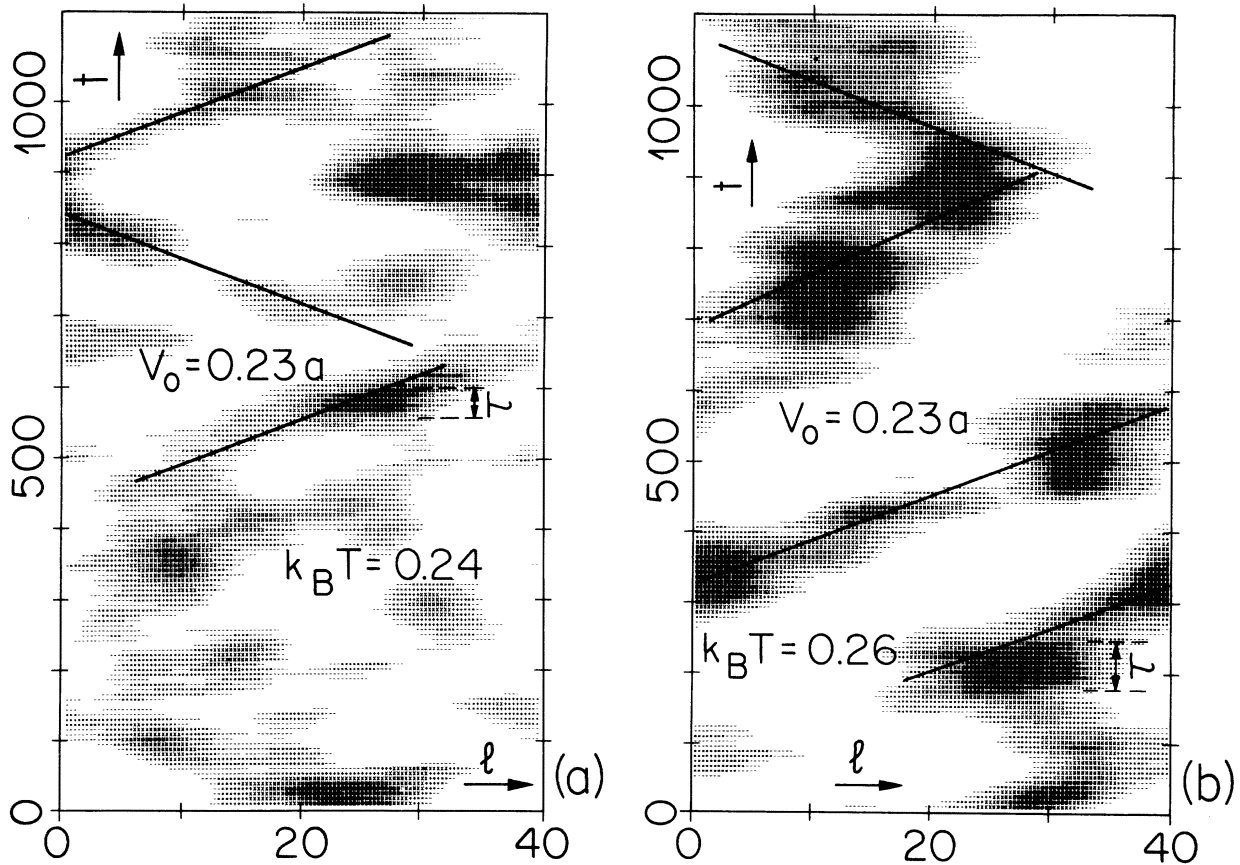


FIG. 18. Hysometric plot of $X_i^*(t)$ [Eq. (60)] for the ferrodistorive model III at (a) $k_B T = 0.24$ and (b) $k_B T = 0.26$. Negative values of X_i^* have been suppressed. Increasing blackening corresponds to increasing displacements. $V_0 = 0.23a$ denotes the mean velocity of the cluster waves, and τ a cluster lifetime.

$X_i^*(t)$ describes the slow fluctuations of the displacement in space (\vec{R}_i) and time, provided that the cut offs k_{xc} and ω_c are sufficiently small. The continuum version of the equation of motion of the ferrodistorptive model [see Eq. (C3)] suggests that traveling-wave solutions

$$X_i(t) = f((\vec{R}_x, 0), t) = f((\vec{R}_x, 0) - (V_x, 0)t) \quad (61)$$

may dominate $X_i^*(t)$, provided that [see Appendix C, Eq. (C6)]

$$m V_x^2 < C a^2. \quad (62)$$

In fact, following Krumhansl and Schrieffer, one can identify these particular solutions as traveling cluster waves (see Appendix C).

In Figs. 18(a) and 18(b), we plotted the calculated $X_i^*(t)$ [Eq. (60)], where negative values have been suppressed, for the ferrodistorptive model III, at $k_B T = 0.24$ and $k_B T = 0.26$, respectively. \vec{k} was chosen along the (1,1) direction excluding $\vec{k} = \vec{0}$. The cut offs are specified in Figs. 19(a) and 19(b). Increasing blackening (Fig. 18) corresponds to increasing displacements. These plots demonstrate, in analogy to Fig. 10, that clusters of locally ordered regions and cluster walls exist. Another important result is that the clusters propagate with a finite lifetime τ and velocity V . At both temperatures, the velocities are distributed around $V_0 = 0.24a$. This value agrees quite well with the group velocities of the new excitation branches shown in Figs. 19(a) and 19(b). Therefore, from these results, one will naturally be led to the conclusion that the new excitations appearing in the ferrodistorptive model III correspond to traveling cluster waves. This result is consistent with the existence of the above-men-

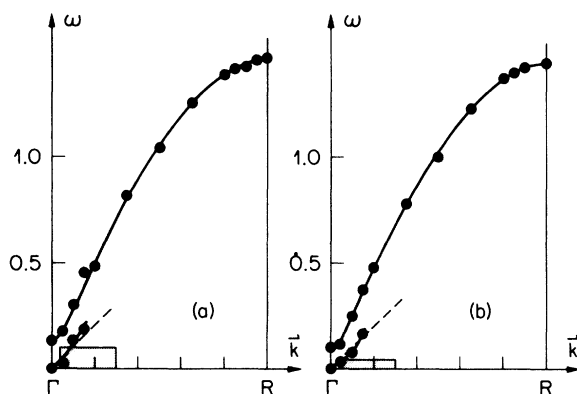


FIG. 19. Calculated dispersion law of the ferrodistorptive model III at (a) $k_B T = 0.24$; (b) $k_B T = 0.26$; we only show the low-lying phonon branch and the new excitation branch. The shadowed rectangle marks the $\omega - \vec{k}$ region over which the sum in Eq. (60) has been performed. The dashed line corresponds to a group velocity of $0.23a$.

tioned particular solutions but by no means guaranteed by the existence of these solutions. In fact, our $X_i^*(t)$ has been calculated for an aged system, or in other words, our $X_i^*(t)$ is independent of the initial conditions.

According to Fig. 20, a similar pattern of $X_i^*(t)$ occurs in model I at $k_B T = 8$ where the new excitation branch also appeared (Fig. 15). The mean cluster wave velocity $V_0 = 0.12a$ and the group velocity derived from Fig. 15(b) again agree quite well.

To investigate the temperature dependence of these cluster waves, we also calculated $X_i^*(t)$ in the ferrodistorptive model at $k_B T = 5.7$, being closer to $k_B T = 5.3$. The results are shown in Fig. 21, and reveal a nearly vanishing mean velocity and a longer lifetime.

Let us now turn to the mechanism underlying the central-peak phenomenon. Recognizing that the cluster waves propagate with a finite lifetime (see Figs. 18, 20, and 21), it is obvious that for small wave vectors \vec{k} , where the frequency of the cluster waves $\omega = V_0 \vec{k}$ is small, the

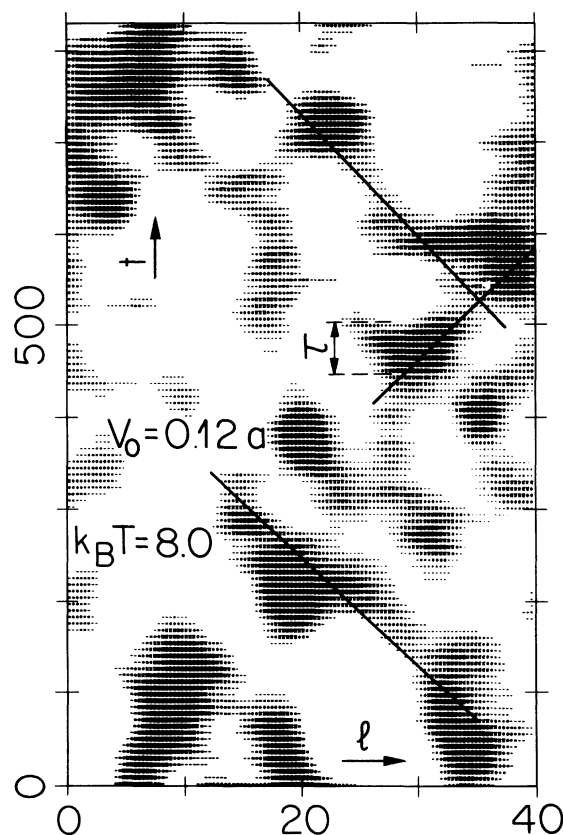


FIG. 20. Hypsometric plot of $X_i^*(t)$ [Eq. (60)] for the ferrodistorptive model I at $k_B T = 8.0$. $V_0 = 0.12a$ denotes the mean velocity, and τ a cluster lifetime.

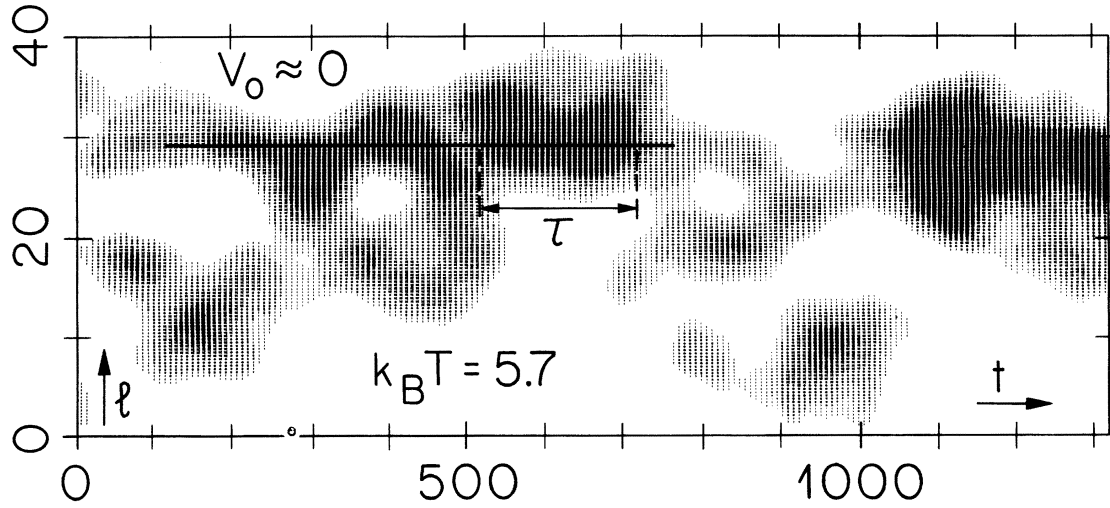


FIG. 21. Hypsometric plot of $X_i^*(t)$ for the ferrodistorptive model I at $k_B T = 5.7$. $V_0 \approx 0$ designates the nearly vanishing mean velocity, and τ a cluster lifetime.

damped cluster waves become overdamped and give rise to the central-peak phenomenon. Here the wave vector \vec{k} is taken relative to the Γ point or R point (Fig. 11). Consequently, the central-peak half-width is proportional to the inverse lifetime of the cluster waves and its height is proportional to this lifetime. For larger \vec{k} values, and in those situations where the cluster waves become underdamped ($V_0 k > 1/\tau$) the central peak splits, which in turn gives rise to the new excitation branch [Figs. 12(b), 13(b), 15(b), and 19].

To summarize this section, we have shown that damped traveling cluster waves exist. Their lifetime was found to increase by approaching T_c and determines the central-peak half-width and height. In fact, the characteristic lifetime of the cluster waves shown in Figs. 18, 20, and 21, are consistent with the corresponding half-widths $\Delta\omega = 1/\tau$ in Figs. 12(a), 13(a), 14, and 15(a). Moreover, the new excitation has been traced back to traveling cluster waves.

It is important to note, however, that the results presented in this section do not necessarily justify the continuum approximation. In fact, our results have been obtained from a lattice model by filtering out the rapidly varying fluctuations in space and time. Consequently, we have taken into account the effects of the short-wavelength and high-frequency fluctuations on the slowly varying fluctuations. This is not the case, however, in the continuum approximation where the short-wavelength fluctuations which may give rise to complicated effects, are neglected. Such effects are that they act as a reservoir causing dissipation,²⁷ and that they may combine to form additional long-wavelength excitations. An interesting ex-

ample is the occurrence of a central peak in the antiferrodistorptive model III around $(\pi/a)(4, 0)$ which must be attributed to two-phonon processes.⁸

E. Critical slowing down

The critical slowing down of a dynamic variable A may be characterized by the characteristic frequency or relaxation time defined by

$$\begin{aligned} \frac{1}{\omega_{AA}(\vec{k})} &= \tau_{AA}(\vec{k}) = \hat{S}_{AA}(\vec{k}, \omega = 0) \\ &= \frac{2 \int_0^\infty S_{AA}(\vec{k}, t) dt}{S_{AA}(\vec{k}, t = 0)}. \end{aligned} \quad (63)$$

If the variable A is not conserved, $\tau_{AA}(\vec{k})$ is expected to diverge at the wavelength \vec{k}_c where $S_{AA}(\vec{k}_c, t = 0)$ diverges according to

$$\frac{1}{\omega_{AA}(\vec{k}_c)} = \tau_{AA}(\vec{k}_c) \sim \left| \frac{T - T_c}{T_c} \right|^{-\Delta_{AA}}. \quad (64)$$

To estimate $\tau_{AA}(\vec{k}_c)$ we used the procedure outlined in Sec. III C, so that our upper integration limit was finite. Nevertheless, for sufficiently long intervals $t_m - t_n$ (Fig. 5), $S_{AA}(\vec{k}_c, t)$ becomes very small and, consequently, the cut off does not lead to serious limitations, as long as T is not too close to T_c . In any case, T_c cannot be reached because the correlation length has to remain smaller than the linear dimension of the system in order to avoid finite size effects.

In Fig. 22, we plotted the calculated temperature dependence of the order-parameter relaxation time, divided by the corresponding susceptibility for model I (Table I). The conventional the-

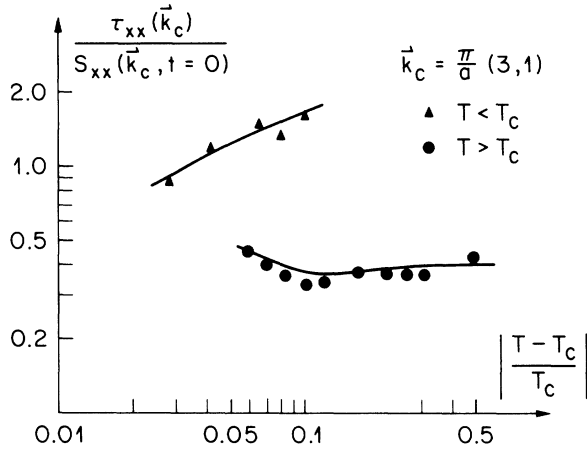


FIG. 22. Temperature dependence of the order-parameter relaxation time [Eq. (63)] divided by the susceptibility $S_{XX}(\vec{k}_c, t=0)$ for model I, at $\vec{k}_c = (\pi/a)(3,1)$.

ory of slowing down predicts that

$$\tau_{xx}(\vec{k}_c)/S_{xx}(\vec{k}_c, t=0) = \text{const} \quad (65)$$

so that

$$\Delta = \gamma. \quad (66)$$

Our results (Fig. 22) reveal that the conventional theory [Eq. (65)] does not hold in the temperature region considered. We note that these results should not be affected by finite size effects, because the correlation length associated with our smallest

$$\left| \frac{T - T_c}{T_c} \right| = 0.03,$$

is still considerably smaller than the linear dimension of our systems.

To elucidate the mechanism underlying this slowing-down phenomenon, we also calculated the

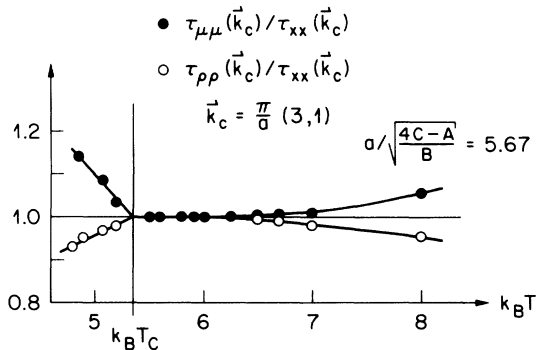


FIG. 23. Temperature dependence of the relaxation-time ratios $\tau_{\mu\mu}(\vec{k}_c)/\tau_{xx}(\vec{k}_c)$ and $\tau_{\rho\rho}(\vec{k}_c)/\tau_{xx}(\vec{k}_c)$ at $\vec{k}_c = (\pi/a)(3,1)$, in model I.

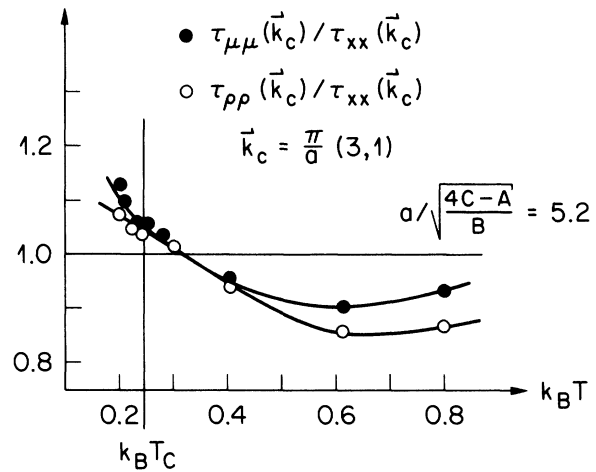


FIG. 24. Temperature dependence of the relaxation-time ratios $\tau_{\mu\mu}(\vec{k}_c)/\tau_{xx}(\vec{k}_c)$ and $\tau_{\rho\rho}(\vec{k}_c)/\tau_{xx}(\vec{k}_c)$ at $\vec{k}_c = (\pi/a)(3,1)$, in model III.

ratios of the relaxation times associated with the Ising spin variable μ , the displacement X , and of the density ρ [Eqs. (44)–(47)]. Figure 23 shows the results for model I, indicating that for $T \rightarrow T_c$, these ratios tend to 1. As Fig. 24 demonstrates, the same behavior was found in model III. Emphasizing again that the Ising spin variable characterizes the formation of clusters and their dynamics, it becomes clear that close to T_c , the cluster dynamics provides the mechanism for the critical slowing down.

V. CONCLUSIONS AND COMMENTS

We have shown that for a one-component model for structural-phase transitions, the molecular-dynamics technique enabling anharmonicity to be treated without drastic approximations, yields useful information about the static and dynamic critical properties provided that the constant-temperature procedure is used. It is clear that this technique has a number of potential applications in the field of phase transitions, and, in particular, a two-component model and tricritical phenomena will be considered in forthcoming publications.

To summarize, our numerical work made it possible to unravel the physical origin of the different motions inherent in a one-component model for structural-phase transitions. On the one hand, each particle undergoes phononlike motions around some momentary position. These motions include the conventional soft-mode phenomena. To understand the other kind of motion one has to realize that the existence of a phase transition is connected with the fact that each par-

ticle also feels an intrinsic (order-disorder regime) or an effective (displacive regime) double-well potential. Thus, as a function of time, the motion of a particle may be decomposed into a slow "flipping" from one well to the other, and comparatively fast oscillations around some displaced instantaneous mean position. An additional feature is that the displacement pattern shows clusters of particles oscillating in the left well together with clusters of the opposite type.

There is no doubt that the two different kinds of motion, phononlike oscillations and collective "flipping" motions, are properties of any *nonisotropic* n -component model Hamiltonian for structural-phase transitions. It should be emphasized, however, that the "flipping" degrees of freedom increase with the number n of the displacement components. In fact, there are $2n$ different cluster patterns for cubic anisotropy.

Recently, molecular-dynamics studies have also been carried out in equivalent but one-dimensional systems which may be related to structural transitions of the so-called Peierls type in pseudo-one-dimensional materials.^{7,28-30} These calculations were performed, however, by means of the conventional microcanonical technique, being unsuitable to investigate critical properties (see Sec. III). In one-dimensional systems such properties occur at $T=0$, where the classical displacement susceptibility diverges. As a consequence, the microcanonical technique can provide only a qualitative picture of the low-temperature properties of these systems. Nevertheless, results equivalent to those found in our two-dimensional systems for $T \geq T_c$ are expected.

Approaches to include the "flipping" motions and their collective appearance in the form of clusters, have recently been put forward by Krumhansl and Schrieffer¹² for the one-dimensional chain, by Bishop and Krumhansl³¹ for coupled arrays of chains, and by Beck³² for a small number of coupled quartic anharmonic oscillators.

Finally, we discuss the connection between the models we have studied and real systems. There is considerable evidence that the static properties of structural-phase transitions are well described by an anisotropic n -component displacement Hamiltonian.³³⁻³⁹ This includes stressed and "monodomain" crystals. Neglecting the kinetic energy of the particles, such Hamiltonians may also be considered as models for magnetic systems, where at each lattice site l there is a spin variable \vec{X}_l with n components. The static critical properties of these model Hamiltonians have been studied rather extensively by means of the renormalization-group technique.^{1,37-39} Even exact results have been established,^{40,41} including

the existence of phase transitions¹⁰ and tricritical points.^{42,43}

Of particular relevance in this context are the results of Aharony and Bruce³⁸ suggesting that under various stress conditions, the critical behavior of the structural transitions in the perovskites SrTiO₃ and LaAlO₃ might be of the Ising, XY, or Heisenberg type and might include a bicritical point with a flop line. The Ising critical behavior occurs by applying an equivalent stress along the (1,0,0) axis. These predictions have recently been well confirmed in SrTiO₃.⁴⁴

It then appears that even the one-component models considered in this work embodies some of the essential features of real systems. Nevertheless one should keep in mind that our model systems are incompressible. In fact, we assumed a rigid reference lattice. Consequently, acoustic modes and their interaction with the order-parameter fluctuations, are lacking in our models. Thus we neglected the effects arising from the interaction between the soft mode, the cluster waves, and the acoustic modes, which is expected to occur in real systems.

Finally we note, that the central peaks in real systems, as observed in $S_{\rho\rho}(\vec{k}, \omega)$ turn out to be much narrower than the central peaks reported here.^{20,21} Recent experiments⁴⁵ suggest that this discrepancy is related to the different dimensionality of the systems. In fact, inelastic neutron-scattering experiments on the high-temperature phase transition of NaNbO₃ indicate that a sharp narrowing of the central peak occurs at the change-over from two- to three-dimensional behavior.

ACKNOWLEDGMENTS

The authors are indebted to H. Beck, Ph. Choquard, J. L. Lebowitz, K. A. Müller, St. Sarbach, and H. Thomas for valuable suggestions on this work.

APPENDIX A: TEST OF THE INTEGRATION AND CONSTANT-TEMPERATURE PROCEDURE

To study the influence of the numerical noise and of the constant-temperature procedure (see Sec. III B), we considered the ferrodistorptive harmonic system defined by

$$\mathcal{H} = \frac{1}{2} \sum_l \left(\dot{X}_l^2 + \dot{Y}_l^2 \right) + \frac{A}{2} \sum_l \left(X_l^2 + Y_l^2 \right) - C \sum_{l,m} X_l Y_{l+m}, \quad (\text{A1})$$

where

$$A = 2.0004, \quad C = 0.5. \quad (\text{A2})$$

Assuming a rigid square reference lattice (Fig. 1), and introducing

$$X(\vec{q}, t) = \frac{1}{N} \sum_i X_i(t) e^{i\vec{q} \cdot \vec{R}_{iX}}, \quad (\text{A3})$$

$$Y(\vec{q}, t) = \frac{1}{N} \sum_i Y_i(t) e^{i\vec{q} \cdot \vec{R}_{iY}},$$

$$U(\vec{q}, t) = X(\vec{q}, t) + Y(\vec{q}, t), \quad (\text{A4})$$

we find from the equation of motion the normal mode frequencies

$$\omega_0^2(\vec{q}) = A \pm 2C \left(\cos a \frac{qx+qy}{2} + \cos a \frac{qx-ay}{2} \right). \quad (\text{A5})$$

The displacement correlation function is then given by

$$\begin{aligned} \hat{S}_0(\vec{q}, t) &= \frac{S_0(\vec{q}, t)}{S_0(\vec{q}, 0)} = \frac{\langle U(-\vec{q}, 0) U(\vec{q}, t) \rangle}{\langle U(-\vec{q}, 0) U(\vec{q}, 0) \rangle} \\ &= \cos \omega_0(\vec{q}) t. \end{aligned} \quad (\text{A6})$$

To compare this exact result with the molecular-dynamics estimate defined by [see Eq. (43)]

$$\hat{S}(\vec{q}, t) = \frac{N}{t_n - t_m - t} \int_{t_m}^{t_n-t} dt' U(-\vec{q}, t') U(\vec{q}, t+t') \quad (\text{A7})$$

we introduce the function

$$\hat{S}_1(\vec{q}, t) = \cos[(\omega_0(\vec{q}) + \Delta\omega(\vec{q}))t] e^{-t/\tau(\vec{q})}, \quad (\text{A8})$$

to estimate the frequency shift and the damping arising in (A7) due to numerical noise and the constant-temperature procedure.

Starting with the initial conditions taken from model III at low temperatures, we switched on the constant-temperature procedure described in Sec. III B, by choosing $k_B T = 0.24$, being close to T_c of model III (Table I). The system was then

aged over 20 000 time steps. The time evolution of the system was then followed over the next 90 000 time steps of unit length 0.02828. The canonical variables of this interval were then used to calculate $\hat{S}(\vec{q}, t)$ [Eq. (A7)] for different wave vectors and time intervals. By comparing the numerical results with Eq. (A8), we also evaluated the frequency shift $\Delta\omega(\vec{q})/\omega_0(\vec{q})$, the damping constant $\tau(\vec{q})$, as well as the root-mean-square deviation

$$\Delta^2(q) = \frac{\int_0^{t_{\max}} [\hat{S}(\vec{q}, t) - \hat{S}_1(\vec{q}, t)]^2 dt}{\int_0^{t_{\max}} [\hat{S}(\vec{q}, t)]^2 dt}. \quad (\text{A9})$$

The results are summarized in Table II. In this context, it is important to note that A and C , specified in Eq. (A2) have been chosen in such a way that $\omega_0(\vec{q})$ at $\vec{q} = (\pi/a)(0, 0)$ corresponds to the half-width of the central peak in model III at $k_B T = 0.24$ [Fig. 12(a)]. Moreover, $\omega_0(\vec{q} = (\pi/a)(2, 0))$ corresponds to the highest normal mode frequency of this system (Fig. 12). It then follows from Table II that the "central-peak half-width" arising from the numerical noise and the constant-temperature procedure, is 10^4 times smaller than the half-width in model III at $k_B T = 0.24$. Consequently, the central peaks observed in our models is not the artifact of the calculation procedure. Moreover, the frequency shift and the root-mean-square deviations are also seen to be negligibly small.

In conclusion, we have shown that time-dependent phenomena can be calculated with rather high accuracy and that the numerical noise and the constant-temperature procedure do not seriously affect our results.

APPENDIX B: THE SELF-CONSISTENT PHONON APPROXIMATION

Here we sketch the important steps in the derivation of the normal mode frequencies within the

TABLE II. Comparison between the exact wave-vector-dependent displacement correlation function of coupled harmonic oscillator and that evaluated by means of the constant-temperature procedure. $\omega_0(\vec{q})$ is the exact normal mode frequency (A5). t_{\max} designates the time interval, $t_{\max}/\Delta t$ designates the number of time steps, $\omega_0(\vec{q}) t_{\max}/2\pi$ designates the number of periods. $\Delta\omega(\vec{q})$ is the frequency shift and $\tau(\vec{q})$ is the damping constant [Eq. (A8)] characterizing the effects of the numerical noise and of the constant-temperature procedure. $\Delta(\vec{q})$ denotes the root-mean-square deviation [Eq. (A9)]. $\omega_0(\vec{q})$ is given by Eq. (A5) with the minus sign.

$\vec{q} \frac{a}{\pi}$	$\omega_0(\vec{q})$	t_{\max}	$\frac{t_{\max}}{\Delta t}$	$\frac{\omega_0(\vec{q}) t_{\max}}{2\pi}$	$\frac{\Delta\omega(\vec{q})}{\omega_0(\vec{q})}$	$\tau(\vec{q}) \omega_0(\vec{q})$	$\Delta(\vec{q})$
(2, 0)	2.0001	424	15 000	135	-1.3×10^{-4}	3.4×10^4	0.16×10^{-2}
(1.5, 0.5)	1.7322	424	15 000	117	-2.0×10^{-4}	4.7×10^4	0.6×10^{-2}
(0.05, 0.05)	0.1127	848	30 000	15	-12.0×10^{-4}	-4.3×10^4	0.11×10^{-2}
(0, 0)	0.02	1696	60 000	5.4	-10.0×10^{-4}	-2.5×10^4	0.7×10^{-2}

framework of the self-consistent phonon approximation (SCPA). First we consider the ferro-distortive model defined by Eqs. (1) and (5). The equation of motion reads

$$-m\ddot{X}_i = AX_i + BX_i^3 - C \sum_m Y_{i+m}, \quad (\text{B1})$$

$$-m\ddot{Y}_i = AY_i + BY_i^3 - C \sum_m X_{i+m}.$$

In the SCPA one replaces

$$\begin{aligned} X_i^3 &\rightarrow 3\langle X_i^2 \rangle X_i, \\ Y_i^3 &\rightarrow 3\langle Y_i^2 \rangle Y_i. \end{aligned} \quad (\text{B2})$$

The normal mode frequencies are then given by

$$m\omega^2(\vec{q}) = A + 3B\langle X_i^2 \rangle \pm 2C[\cos\frac{1}{2}a(q_x + q_y) + \cos\frac{1}{2}a(q_x - q_y)]. \quad (\text{B3})$$

In the antiferrodistortive model, we find below T_c

$$\omega^2(\vec{q}) = A + 3B\langle X_i^2 \rangle \pm 2C[\cos\frac{1}{2}a(q_x + q_y) \pm \cos\frac{1}{2}a(q_x - q_y)] \quad (\text{B4})$$

and above T_c

$$\omega^2(\vec{q}) = A + 3B\langle X_i^2 \rangle \pm 2C[\cos\frac{1}{2}a(q_x + q_y) - \cos\frac{1}{2}a(q_x - q_y)]. \quad (\text{B5})$$

$\langle X_i^2 \rangle$ has to be determined self-consistently. For our purpose it was more convenient to use for $\langle X_i^2 \rangle$ the molecular-dynamics results (see Fig. 9).

APPENDIX C: TRAVELING-WAVE SOLUTIONS IN THE CONTINUUM LIMIT

To substantiate the possible importance of cluster waves, we consider the ferrodistorptive model defined by Eqs. (1) and (5) in the continuum limit

$$\begin{aligned} \mathcal{H} = & \frac{m}{2} \sum_i (\dot{X}_i^2 + \dot{Y}_i^2) + \frac{A-4C}{2} \sum_i (X_i^2 + Y_i^2) \\ & + \frac{B}{4} \sum_i (X_i^4 + Y_i^4) + \frac{C}{2} \sum_{i,m} (X_i - Y_{i+m})^2. \end{aligned} \quad (\text{C1})$$

Introducing the displacement field $f(\vec{R})$, (C1) reduces in the continuum limit to

$$\begin{aligned} \mathcal{H} = & \int d^2R \left(\frac{m}{2} \dot{f}^2(\vec{R}) + \frac{A-4C}{2} f^2(R) + \frac{B}{4} f^4(\vec{R}) \right. \\ & \left. + \frac{Ca^2}{2} [\nabla f(\vec{R})]^2 \right). \end{aligned} \quad (\text{C2})$$

The equation of motion becomes

$$-m\ddot{f}(\vec{R}, t) = (A-4C)f(\vec{R}, t) + Bf^3(\vec{R}, t) - Ca^2\Delta f(\vec{R}, t). \quad (\text{C3})$$

Traveling-wave solutions can be obtained by assuming

$$f(\vec{R}, t) = f(\vec{R} - \vec{V}t). \quad (\text{C4})$$

\vec{V} denotes the wave velocity. For our purpose it is sufficient to consider waves propagating along the X direction,

$$f(R_x, 0, t) = f(R_x, 0) - (V_x, 0)t. \quad (\text{C5})$$

The resulting particular solutions of (C3) reduce to that considered by Krumhansl and Schrieffer.¹² Of particular relevance in our context are the solutions with

$$mV_x^2 < Ca^2. \quad (\text{C6})$$

An example is

$$f(R_x, t) = \left(\frac{4C-A}{B} \right)^{1/2} \tanh\left(\frac{R_x - V_x t}{\xi_x \sqrt{2}} \right), \quad (\text{C7})$$

$$\xi_x^2 = \frac{Ca^2 - V_x^2 m}{4C-A}. \quad (\text{C8})$$

Over the semi-infinite region $R_x - V_x t < 0$ the displacement field is constant and given by the negative value of the zero-temperature order parameter [Eq. (3)]. For $R_x - V_x t > 0$, however, the displacement equals the positive value of the zero-temperature order parameter. The transition takes place through a cluster wall of approximate thickness $2\sqrt{2}\xi_x$. The wall moves with V_x .

¹M. E. Fisher, Rev. Mod. Phys. **46**, 597 (1974).

²S. Sarbach, T. Schneider, and E. Stoll, Phys. Rev. B **10**, 2004 (1974).

³A. Rahman, Phys. Rev. **136**, A405 (1964).

⁴L. Verlet, Phys. Rev. **159**, 98 (1967).

⁵T. Schneider and E. Stoll, Phys. Rev. Lett. **31**, 1254 (1973).

⁶T. Schneider and E. Stoll, in *Local Properties at Phase Transitions*, edited by K. A. Müller and A. Rigamonti (Academic, New York, to be published).

⁷T. Schneider and E. Stoll, Phys. Rev. Lett. **30**, 296 (1975).

⁸T. Schneider and E. Stoll, J. Phys. C **8**, 283 (1975).

⁹T. Schneider and E. Stoll, Phys. Rev. B **10**, 4799 (1974).

¹⁰H. Kunz and B. Payandeh (unpublished).

¹¹F. Schwabl, in *Anharmonic Lattices, Structural Transition and Melting*, edited by T. Riste (Leiden, Noordhoff, 1974), p. 87.

¹²J. A. Krumhansl and J. R. Schrieffer, Phys. Rev. B **11**,

- 3535 (1975).
- ¹³H. Beck, T. Schneider, and E. Stoll, *Phys. Rev. B* **12**, 5198 (1975).
- ¹⁴C. W. Gear, ANL Report No. ANL-7126 (1966) (unpublished).
- ¹⁵J. L. Lebowitz, J. K. Percus, and L. Verlet, *Phys. Rev.* **153**, 250 (1967).
- ¹⁶M. E. Fisher, *Rep. Prog. Phys.* **30**, 615 (1967).
- ¹⁷Th. von Waldkirch, K. A. Müller, and W. Berlinger, *Phys. Rev. B* **7**, 1052 (1973).
- ¹⁸This film is available from the authors on request.
- ¹⁹For a review and references see W. Cochran, in *Structural Phase Transitions and Soft Modes*, edited by E. J. Samuelsen, E. Anderson, and J. Feder (Universitetsforlaget, Oslo, 1971), p. 1.
- ²⁰S. M. Shapiro, J. P. Axe, A. Shirane, and T. Riste, in Ref. 11, p. 135.
- ²¹K. A. Müller, W. Berlinger, C. West, and P. Heller, *Phys. Rev. Lett.* **32**, 160 (1974).
- ²²G. F. Reiter, W. Berlinger, T. Schneider, and K. A. Müller, in *Proceedings of the Eighteenth Ampere Congress Nottingham*, edited by P. S. Allen, E. R. Andrew, and C. A. Bates (North-Holland, Amsterdam, 1975), Vol. II, p. 309.
- ²³K. K. Murata, *Phys. Rev. B* **11**, 462 (1975).
- ²⁴B. B. Kadomtsev and V. I. Karpan, *Usp. Fiz. Nauk* **103**, 193 (1971) [*Sov. Phys.-Usp.* **14**, 40 (1971)].
- ²⁵A. C. Scott, F. Y. F. Chu, and P. W. McLaughlin, *Proc. IEEE* **61**, 1443 (1973).
- ²⁶G. M. Zaslavskii, *Usp. Fiz. Nauk* **111**, 395 (1973) [*Sov. Phys.-Usp.* **16**, 761 (1974)].
- ²⁷T. Schneider and E. Simanek, *J. Phys. C* **8**, 1633 (1975).
- ²⁸S. Aubry and R. Pick, *Ferroelectrics* **8**, 471 (1974).
- ²⁹S. Aubry, *J. Chem. Phys.* **62**, 3217 (1975).
- ³⁰T. R. Koehler, A. R. Bishop, J. A. Krumhansl, and J. R. Schrieffer, *Solid State Commun.* (to be published).
- ³¹A. R. Bishop and J. A. Krumhansl (unpublished).
- ³²H. Beck (unpublished).
- ³³K. A. Müller, W. Berlinger, and J. C. Slonczewski, *Phys. Rev. Lett.* **25**, 734 (1970).
- ³⁴J. C. Slonczewski and H. Thomas, *Phys. Rev. B* **1**, 3599 (1970).
- ³⁵J. C. Slonczewski, *Phys. Rev. B* **2**, 4646 (1970).
- ³⁶K. A. Müller and W. Berlinger, *Phys. Rev. Lett.* **26**, 13 (1971).
- ³⁷R. A. Cowley and A. D. Bruce, *J. Phys. C* **6**, 191 (1973).
- ³⁸A. Aharony and A. D. Bruce, *Phys. Rev. Lett.* **33**, 427 (1974).
- ³⁹D. Mukamel, *Phys. Rev. Lett.* **34**, 481 (1975).
- ⁴⁰L. Sasvari and P. Szeffalussy, *J. Phys. C* **7**, 1061 (1974).
- ⁴¹T. Schneider, E. Stoll, and H. Beck, *Physica* **79A**, 201 (1975).
- ⁴²V. J. Emery, *Phys. Rev. B* **11**, 3397 (1975).
- ⁴³S. Sarbach and T. Schneider, *Z. Phys. B* **20**, 399 (1975).
- ⁴⁴K. A. Müller and W. Berlinger (private communication).
- ⁴⁵R. Comes, R. Currat, F. Denoyer, M. Lambert, and A. M. Quittet (unpublished).

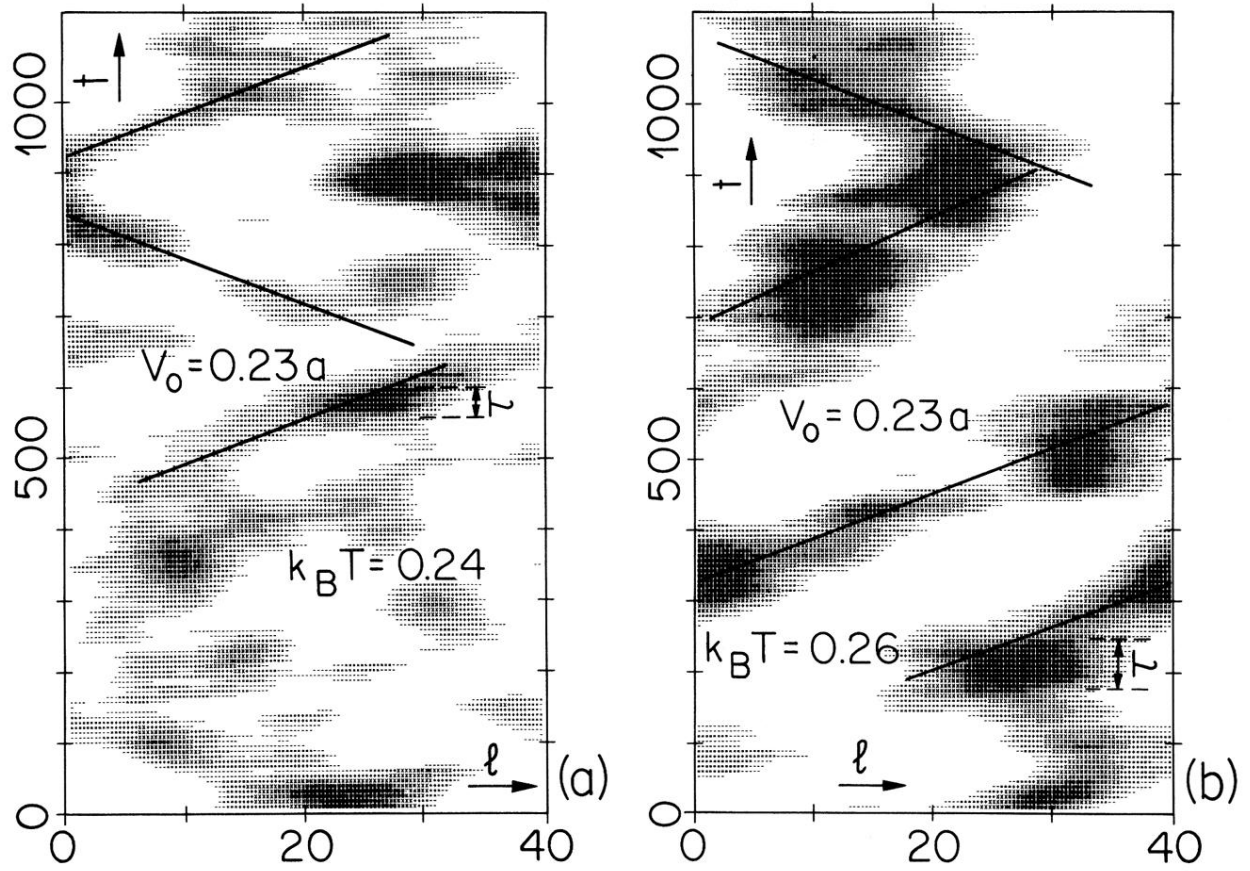


FIG. 18. Hysometric plot of $X_i^*(t)$ [Eq. (60)] for the ferrodistorptive model III at (a) $k_B T = 0.24$ and (b) $k_B T = 0.26$. Negative values of X_i^* have been suppressed. Increasing blackening corresponds to increasing displacements. $V_0 = 0.23a$ denotes the mean velocity of the cluster waves, and τ a cluster lifetime.

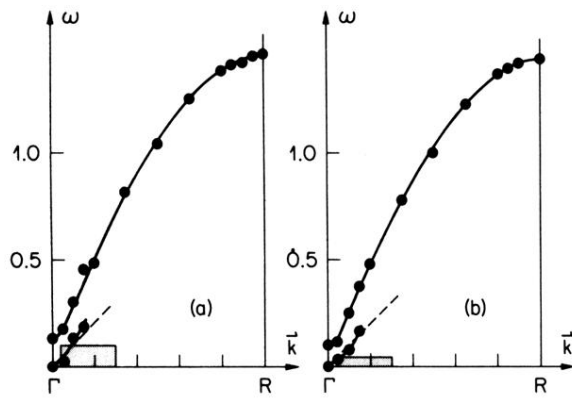


FIG. 19. Calculated dispersion law of the ferrodis-tortive model III at (a) $k_B T = 0.24$; (b) $k_B T = 0.26$; we only show the low-lying phonon branch and the new excitation branch. The shadowed rectangle marks the $\omega - \vec{k}$ region over which the sum in Eq. (60) has been performed. The dashed line corresponds to a group velocity of $0.23a$.

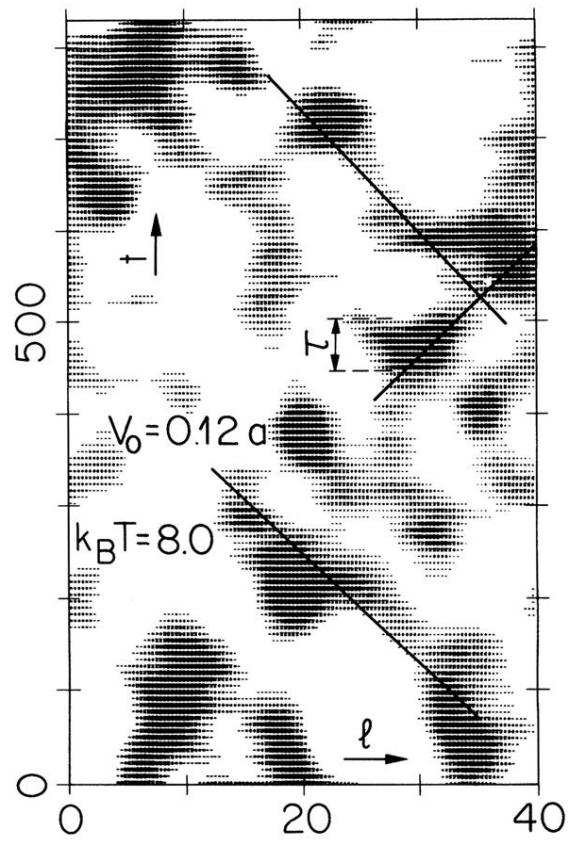


FIG. 20. Hypsometric plot of $X_i^*(t)$ [Eq. (60)] for the ferrodistorptive model I at $k_B T = 8.0$. $V_0 = 0.12 a$ denotes the mean velocity, and τ a cluster lifetime.

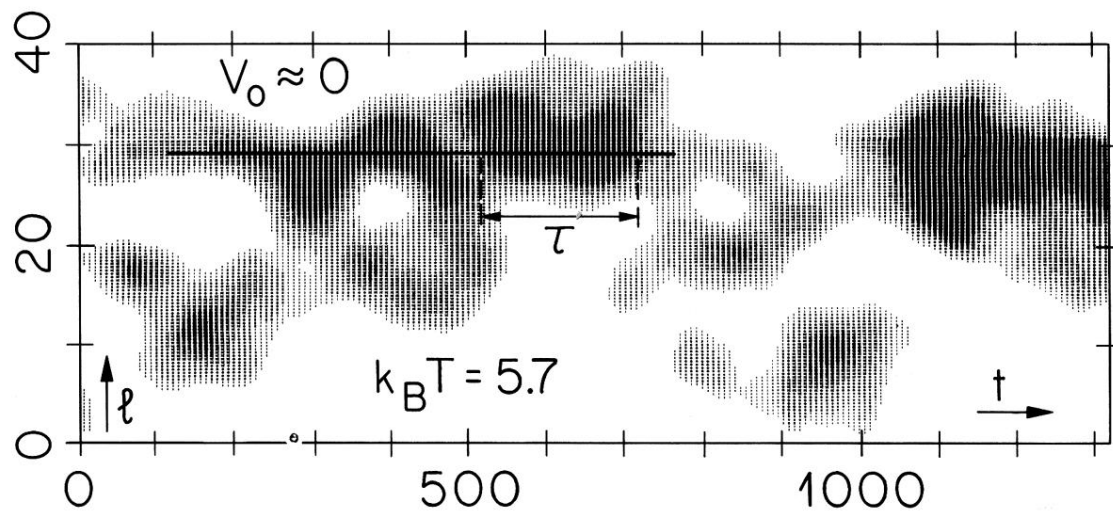


FIG. 21. Hypsometric plot of $X_i^*(t)$ for the ferrodistorptive model I at $k_B T = 5.7$. $V_0 \approx 0$ designates the nearly vanishing mean velocity, and τ a cluster lifetime.